PDGFRα signaling regulates Srsf3 transcript binding to affect PI3K signaling and endosomal trafficking

Thomas E. Forman[1,2], Marcin P. Sajek[3,4,5], Eric D. Larson[6,7], Neelanjan Mukherjee[3,4], Katherine A. Fantauzzo[1,4,*]

[1]Department of Craniofacial Biology, School of Dental Medicine, University of Colorado Anschutz Medical Campus, Aurora, CO, USA

[2]Medical Scientist Training Program, University of Colorado Anschutz Medical Campus, Aurora, CO, USA

[3]Department of Biochemistry and Molecular Genetics, School of Medicine, University of Colorado Anschutz Medical Campus, Aurora, CO, USA

[4]RNA Bioscience Initiative, University of Colorado Anschutz Medical Campus, Aurora, CO, USA

[5]Institute of Human Genetics, Polish Academy of Sciences, Poznan, Poland

[6]Department of Otolaryngology – Head and Neck Surgery, University of Colorado Anschutz Medical Campus, Aurora, CO, USA

[7]Basic and Translational Sciences, Penn Dental Medicine, University of Pennsylvania, Philadelphia, PA, USA

*Corresponding author. Email: katherine.fantauzzo@cuanschutz.edu

Abstract

Signaling through the platelet-derived growth factor receptor alpha (PDGFRα) plays a critical role in craniofacial development, as mutations in *PDGFRA* are associated with cleft lip/palate in humans and *Pdgfra* mutant mouse models display varying degrees of facial clefting. Phosphatidylinositol 3-kinase (PI3K)/Akt is the primary effector of PDGFRα signaling during skeletal development in the mouse. We previously demonstrated that Akt phosphorylates the RNA-binding protein serine/arginine-rich splicing factor 3 (Srsf3) downstream of PI3K-mediated PDGFRα signaling in mouse embryonic palatal mesenchyme (MEPM) cells, leading to its nuclear translocation. We further showed that ablation of *Srsf3* in the murine neural crest lineage results in severe midline facial clefting, due to defects in proliferation and survival of cranial neural crest cells, and widespread alternative RNA splicing (AS) changes. Here, we sought to determine the molecular mechanisms by which Srsf3 activity is regulated downstream of PDGFRα signaling to control AS of transcripts necessary for craniofacial development. We demonstrated via enhanced UV-crosslinking and immunoprecipitation (eCLIP) of MEPM cells that PDGF-AA stimulation leads to preferential binding of Srsf3 to exons and loss of binding to canonical Srsf3 CA-rich motifs. Through the analysis of complementary RNA-seq data, we showed that Srsf3 activity results in the preferential inclusion of exons with increased GC content and lower intron to exon length ratio. Moreover, we found that the subset of transcripts that are bound by Srsf3 and undergo AS upon PDGFRα signaling commonly encode regulators of PI3K signaling and early endosomal trafficking. Functional validation studies further confirmed that Srsf3 activity downstream of PDGFRα signaling leads to retention of the receptor in early endosomes and increases in downstream PI3K-mediated Akt signaling. Taken together, our findings reveal that growth factor-mediated phosphorylation of an RNA-binding protein underlies gene expression regulation necessary for mammalian craniofacial development.

45 **Introduction**

46 Craniofacial development is a complex morphogenetic process that requires a precise
47 interplay of multiple cell and tissue types to generate the frontonasal skeleton. Disruption of this
48 process can result in some of the most common birth defects in humans, such as cleft lip and
49 palate (Mai et al., 2019). Signaling through the platelet derived growth factor receptor alpha
50 (PDGFRα) receptor tyrosine kinase (RTK) is essential for human craniofacial development.
51 Heterozygous missense mutations in the coding region of *PDGFRA* that alter amino acids within
52 the extracellular, transmembrane or cytoplasmic domains of the receptor, in addition to single
53 base-pair substitutions in the 3' untranslated region (3' UTR), are associated with nonsyndromic
54 cleft palate (Rattanasopha et al., 2012). Further, single-nucleotide polymorphisms that repress
55 transcriptional activity of the promoter upstream of *PDGFC*, which encodes one of two PDGFRα
56 ligands, are associated with cleft lip and palate (Choi et al., 2009). This role of PDGFRα
57 signaling in craniofacial development is conserved in mice, as *Pdgfra* mutant mouse models
58 display a variety of defects that range from cleft palate to complete facial clefting (Klinghoffer et
59 al., 2002; Soriano, 1997; Tallquist & Soriano, 2003; Fantauzzo & Soriano, 2014; He & Soriano,
60 2013). These phenotypes are recapitulated in embryos lacking both *Pdgfa* and *Pdgfc* (Ding et
61 al., 2004). Phosphatidylinositol 3-kinase (PI3K) is the primary effector of PDGFRα signaling
62 during skeletal development in the mouse (Klinghoffer et al., 2002). Following activation, PI3K
63 increases phosphatidylinositol-3,4,5-trisphosphate (PIP_3) levels at the cell membrane, leading to
64 the recruitment and subsequent phosphorylation of the serine/threonine kinase Akt. Akt
65 subsequently dissociates from the membrane to phosphorylate an array of target proteins that
66 are involved in wide-ranging cellular processes (Manning & Cantley, 2007). We previously
67 identified proteins phosphorylated by Akt downstream of PI3K-mediated PDGFRα signaling in
68 primary mouse embryonic mesenchyme (MEPM) cells (Fantauzzo & Soriano, 2014). Gene

69 ontology analysis revealed that 25% of the 56 proteins were involved in RNA processing, with a
70 particular enrichment for RNA splicing (Fantauzzo & Soriano, 2014).

71 Alternative RNA splicing (AS) is a process by which different combinations of exons from
72 the same gene are incorporated into mature RNA transcripts, thereby contributing to gene
73 expression regulation and enhancing the diversity of protein isoforms (Licatalosi & Darnell,
74 2010). AS occurs in approximately 95% of multi-exon human genes, frequently in a tissue-
75 specific manner (Pan et al., 2008; Wang et al., 2008). Dysregulation of AS causes a number of
76 diseases, due to mutations in precursor RNA sequences, mutations in core components of the
77 spliceosome complex and/or mutations in auxiliary RNA-binding proteins (RBPs) (Scotti &
78 Swanson, 2016). These *trans*-acting auxiliary RBPs bind to specific sequence and/or structural
79 motifs in a target RNA via one or more RNA-binding domains to promote or inhibit exon
80 inclusion (Fu & Ares, 2014; Licatalosi & Darnell, 2010). The phenotypes resulting from global
81 and/or tissue-specific knockout of multiple RBPs have established that RBP-mediated AS is an
82 essential process during mouse craniofacial development (Bebee et al., 2015; Cibi et al., 2019;
83 Dennison et al., 2021; Forman et al., 2021; Lee et al., 2020). We previously demonstrated that
84 ablation of *Srsf3* in the murine neural crest lineage results in severe midline facial clefting and
85 facial bone hypoplasia, due to defects in proliferation and survival of cranial neural crest cells,
86 and widespread AS changes (Dennison et al., 2021).

87 Srsf3 belongs to the serine/arginine-rich (SR) protein family of splicing factors that
88 generally promote exon inclusion by binding to exonic and intronic splicing enhancers and by
89 recruiting spliceosome components to the 5' and 3' splice sites (Fu & Ares, 2014; Licatalosi &
90 Darnell, 2010). Srsf3 specifically was shown to bind pyrimidine-rich motifs, with a preference for
91 exonic regions (Akerman et al., 2009; Änkö et al., 2012). Srsf3 is phosphorylated downstream of
92 PDGF and EGF stimulation and all-*trans* retinoic acid treatment, and by the kinases Akt and
93 SRPK2 (Bavelloni et al., 2014; Dennison et al., 2021; Fantauzzo & Soriano, 2014; Long et al.,
94 2019; Zhou et al., 2012). Phosphorylation of the Akt consensus sites within the C-terminal

95 arginine/serine-rich (RS) domain of Srsf3 drives its translocation to the nucleus, where AS takes
96 place (Bavelloni et al., 2014; Dennison et al., 2021; Long et al., 2019). Moreover,
97 phosphorylation of the RS domain can alter the ability of SR proteins to interact with other
98 proteins, such as the U1 small nuclear ribonucleoprotein (snRNP) component of the
99 spliceosome and additional RBPs, and affect the ability of SR proteins to bind RNA (Huang et
100 al., 2004; Shen & Green, 2006; Shin et al., 2004; Xiao & Manley, 1997). However, the molecular
101 mechanisms by which Srsf3 activity is regulated downstream of specific signaling inputs in a
102 context-specific manner to regulate RNA binding and/or sequence specificity remain
103 undetermined.

104 Here, we identified changes in Srsf3-dependent AS and Srsf3 transcript binding in the
105 absence or presence of PDGF-AA ligand in MEPM cells. RNA-sequencing (RNA-seq) analysis
106 revealed that Srsf3 activity and PDGFRα signaling have more pronounced effects on AS than
107 gene expression, as well as a significant dependence in regulating AS. Using enhanced UV-
108 crosslinking and immunoprecipitation (eCLIP), we found a shift from intronic to exonic Srsf3
109 binding and loss of CA-rich sites upon PDGF-AA stimulation. Further, we demonstrated that the
110 subset of transcripts that are bound by Srsf3 and undergo AS upon PDGFRα signaling
111 commonly encode regulators of PI3K signaling and early endosomal trafficking, ultimately
112 serving as a feedback mechanism to affect trafficking of the receptors. Combined, our findings
113 provide significant insight into the mechanisms underlying RBP-mediated gene expression
114 regulation in response to growth factor stimulation within the embryonic mesenchyme.
115

116 **Results**

117 *PDGFRα signaling for one hour minimally affects gene expression*

118 To determine the Srsf3-dependent changes in gene expression and AS downstream of
119 PDGFRα signaling, we stably integrated a scramble shRNA (scramble) or an shRNA targeting

120 the 3' UTR of *Srsf3* (shSrsf3) into immortalized MEPM (iMEPM) cells via lentiviral transduction
121 (Fig. 1A). Western blotting revealed a 66% decrease in Srsf3 protein levels in the shSrsf3 cell
122 line (Fig. 1B). We previously demonstrated that phosphorylated Srsf3 levels peaked in the
123 nucleus of iMEPM cells following 1 hour of PDGF-AA ligand treatment (Dennison et al., 2021).
124 As such, cells were left unstimulated (-PDGF-AA) or treated with 10 ng/mL PDGF-AA for 1 hour
125 (+PDGF-AA). RNA was isolated and sequenced from three biological replicates across each of
126 the four conditions (Fig. 1A; Table S1). We first examined Srsf3-dependent differentially-
127 expressed (DE) genes by comparing scramble versus shSrsf3 samples across the same PDGF-
128 AA stimulation condition (-PDGF-AA or +PDGF-AA). We detected 827 DE genes in the absence
129 of ligand treatment and 802 DE genes upon ligand stimulation (Fig. 1C, Table S2). There was
130 high overlap (1,042 out of 1,629; 64.0%) of DE genes across ligand treatment conditions (Fig.
131 1C,D; Fig. S1A). Of these 521 shared DE genes, 514 (98.7%) had the same directionality,
132 including 273 (52%) with shared increases in expression in the shSrsf3 samples and 241 (46%)
133 with shared decreases in expression in the shSrsf3 samples (Fig. 1C,D). These findings
134 demonstrate that expression of a set of genes (521) depends on Srsf3 activity independent of
135 PDGFRα signaling, while a similarly sized set of genes (587) is differentially expressed in
136 response to both Srsf3 activity and PDGFRα signaling (Fig. 1C,D). Gene ontology (GO)
137 analysis of the Srsf3-dependent DE genes revealed that the most significant terms for biological
138 process commonly involved regulation of osteoblast differentiation, calcium-dependent cell-cell
139 adhesion, regulation of cell migration and canonical Wnt signaling, while only a handful of
140 significant terms for molecular function were detected in unstimulated cells, relating to cation
141 channel activity and phosphatase activity (Fig. S2A,B).
142 We next examined PDGF-AA-dependent DE genes by comparing -PDGF-AA versus
143 +PDGF-AA across the same Srsf3 condition (scramble or shSrsf3). We detected only 37 DE
144 genes in scramble cells and 14 DE genes in shSrsf3 cells (Fig. 1E, Table S2). There was low

145 overlap (8 out of 51; 15.7%) of DE genes across Srsf3 conditions (Fig. 1E,F; Fig. S1B). Of these
146 4 shared DE genes, 3 (75%) had shared increases in expression upon PDGF-AA stimulation
147 (Fig. 1E,F). These findings demonstrate that, unlike Srsf3 activity, PDGFRα signaling minimally
148 affects gene expression at one hour of ligand stimulation, consistent with our previous findings
149 in mouse embryonic facial mesenchyme (Dennison et al., 2021). Further, these results show
150 that expression of a set of genes (4) depends on PDGFRα signaling independent of Srsf3
151 activity, while a larger set of genes (43) is differentially expressed in response to both PDGFRα
152 signaling and Srsf3 activity (Fig. 1E,F). GO analysis of the PDGF-AA-dependent DE genes
153 revealed significant terms for biological process in the scramble cells relating to cell migration,
154 response to growth factor stimulation and regulation of transcription (Fig. S2A). The most
155 significant terms for molecular function commonly involved DNA binding (Fig. S2B).
156
157 *PDGFRα signaling for one hour has a more pronounced effect on alternative RNA splicing*
158 We previously demonstrated that AS is an important mechanism of gene expression
159 regulation downstream of PI3K/Akt-mediated PDGFRα signaling in the murine mid-gestation
160 palatal shelves (Dennison et al., 2021). Accordingly, we next assessed AS in our same RNA-
161 seq dataset. In examining Srsf3-dependent alternatively-spliced transcripts, we detected 1,354
162 differential AS events in the absence of ligand treatment and 1,071 differential AS events upon
163 ligand stimulation (Fig. 2A). When filtered to include events detected in at least 10 reads in
164 either condition, we obtained a list of 1,113 differential AS events in the absence of ligand
165 treatment and 795 differential AS events upon ligand stimulation (Fig. 2B, Tables S3 and S4).
166 There was low overlap (406 out of 1,908; 21.3%) of alternatively-spliced transcripts across
167 ligand treatment conditions. Of these 203 shared alternatively-spliced transcripts, 100% had the
168 same directionality, including 81 (40%) with shared negative changes in percent spliced in (PSI)
169 (exon included more often in shSrsf3 samples) and 122 (60%) with shared positive changes in

170 PSI (exon skipped more often in shSrsf3 samples) (Fig. 2A,B). We confirmed the differential AS
171 of two transcripts, *Arhgap12* and *Cep55*, between scramble and shSrsf3 samples by qPCR
172 using primers within constitutively-expressed exons flanking the alternatively-spliced exon (Fig.
173 S3A,B). These findings demonstrate that AS of a set of transcripts (203) depends on Srsf3
174 activity independent of PDGFRα signaling, while a much larger set of transcripts (1,502) is
175 alternatively spliced in response to both Srsf3 activity and PDGFRα signaling (Fig. 2A,B). GO
176 analysis of these Srsf3-dependent alternatively-spliced transcripts revealed that the most
177 significant terms for biological process and molecular function commonly involved regulation of
178 RNA splicing, and RNA binding and cadherin binding, respectively (Fig. S4A,B).
179 In examining PDGF-AA-dependent alternatively-spliced transcripts, we detected 595
180 differential AS events in scramble cells and 398 differential AS events in shSrsf3 cells (Fig. 2C).
181 When filtered to include events detected in at least 10 reads in either condition, we obtained a
182 list of 375 differential AS events in scramble cells and 256 differential AS events in shSrsf3 cells
183 (Fig. 2D, Tables S5 and S6). There was extremely low overlap (18 out of 631; 2.85%) of
184 alternatively-spliced transcripts across Srsf3 conditions (Fig. 2C,D). Of these 9 shared
185 alternatively-spliced transcripts, 100% had the same directionality, including 5 (56%) with
186 shared negative changes in PSI (exon included more often in +PDGF-AA samples) and 4 (44%)
187 with shared positive changes in PSI (exon skipped more often in +PDGF-AA samples) (Fig.
188 2C,D). Taken together, these findings demonstrate that both Srsf3 activity and PDGFRα
189 signaling have more pronounced effects on AS than gene expression. While more transcripts
190 and genes are subject to these regulatory mechanisms upon loss of Srsf3 activity, the
191 magnitude of events is more greatly skewed towards AS upon PDGF-AA stimulation. Further,
192 these results show that AS of a set of transcripts (9) depends on PDGFRα signaling
193 independent of Srsf3 activity, while a much larger set of transcripts (613) is alternatively spliced
194 in response to both PDGFRα signaling and Srsf3 activity (Fig. 2C,D). When combined with the

195 data above (Fig. 2B), this points to a profound dependence between PDGFRα signaling and
196 Srsf3 in regulating AS of transcripts in the facial mesenchyme. GO analysis of these PDGF-AA-
197 dependent alternatively-spliced transcripts demonstrated only a handful of significant terms for
198 molecular function in the scramble cells, all relating to protein kinase activity (Fig. S4B).
199 The vast majority of Srsf3-dependent (70.2-73.7%) and PDGF-AA dependent (62.1-
200 65.1%) AS events involved skipped exons, with minimal contribution from retained introns,
201 mutually exclusive exons, alternative 5' splice sites, or alternative 3' splice sites (Fig. 2E). For
202 the Srsf3-dependent skipped exon events, there were more transcripts with +ΔPSI (exon
203 skipped more often in shSrsf3 samples) (44.8%) as opposed to -ΔPSI (exon included more
204 often in shSrsf3 samples) (25.4%) in the absence of PDGF-AA stimulation (Fig. 2E), consistent
205 with previous results that SR proteins tend to promote exon inclusion (Fu & Ares, 2014;
206 Licatalosi & Darnell, 2010). However, PDGF-AA ligand treatment led to an increase in the
207 percentage of transcripts with -ΔPSI (36.5%) (Fig. 2E), indicating that PDGFRα signaling
208 promotes exon skipping in the presence of Srsf3. Among the PDGF-AA-dependent skipped
209 exon events, there was a significant shift in transcripts with -ΔPSI (exon included more often in
210 +PDGF-AA samples) in the absence (41.0%) versus presence (19.5%) of Srsf3, and a
211 corresponding shift in transcripts with +ΔPSI (exon skipped more often in +PDGF-AA samples)
212 (21.1% and 45.6%, respectively) (Fig. 2E), again suggesting that PDGF-AA stimulation causes
213 increased exon skipping when Srsf3 is present.
214
215 *Srsf3 exhibits differential transcript binding upon PDGFRα signaling*
216 To determine direct binding targets of Srsf3 downstream of PDGFRα signaling, we
217 conducted eCLIP (Van Nostrand et al., 2016, 2017) of iMEPM cells that were left unstimulated (-
218 PDGF-AA) or treated with 10 ng/mL PDGF-AA for 1 hour (+PDGF-AA) as above (Fig. 3A; Table
219 S7). Immunoprecipitation with a previously validated Srsf3 antibody (Dennison et al., 2021)

220 successfully enriched for Srsf3 in UV-crosslinked cells (Fig. 3B). We detected 6,555 total eCLIP
221 peaks in protein-coding genes in the -PDGF-AA samples and 8,584 total peaks in the +PDGF-
222 AA samples (Table S8). Among the -PDGF-AA peaks, 3,727 (56.9%) were located in exons
223 (CDS) and 1,690 (25.8%) were located within introns, with the rest binding within 5' UTRs (768,
224 11.7%) and 3' UTRs (367, 5.60%) (Fig. 3C,D; Table S9). We observed substantial shifts in
225 Srsf3-bound regions upon PDGF-AA stimulation. Many more +PDGF-AA peaks were located
226 within exons (7,139, 83.2%), and less were located within introns (765, 8.91%), 5' UTRs (389,
227 4.53%) and 3' UTRs (287, 3.34%) (Fig. 3C,D; Table S9). Given that SR proteins are crucial for
228 exon definition and bind to exonic splicing enhancers to recruit and stabilize core splicing
229 machinery (Fu & Maniatis, 1990; Krainer et al., 1991; Zahler et al., 1993), we investigated Srsf3
230 binding around 5' and 3' splice sites in response to PDGFRα signaling. Consistent with the
231 results above and previous findings (Änkö et al., 2012), Srsf3 binding was enriched in exonic
232 regions, as opposed to intronic regions, surrounding the splice sites (Fig. 3E). There was
233 greater mean coverage of Srsf3 peaks in the +PDGF-AA condition versus the -PDGF-AA
234 condition within 100 nucleotides upstream of the 5' splice site and within 100 nucleotides
235 downstream of the 3' splice site (Fig. 3E). Additionally, we detected decreased mean coverage
236 in the +PDGF-AA condition within 25 nucleotides downstream of the 5' splice site boundary
237 (Fig. 3E). Taken together, these data show that PDGFRα signaling leads to increased binding of
238 Srsf3 to exons. Finally, we performed unbiased motif enrichment analysis of Srsf3 peaks in
239 unstimulated and PDGF-AA-treated samples, revealing that the mostly highly enriched motifs in
240 -PDGF-AA samples were CACACA and AAGAAG (Fig. 3F). Of note, these CA-rich motifs have
241 previously been identified as canonical Srsf3 motifs in a CLIP study utilizing a stably integrated
242 SRSF3-EGFP transgene (Änkö et al., 2012). However, in PDGF-AA-stimulated samples, the
243 most highly enriched motifs were GAAGCG, GAAGAA, and AGAAGA (Fig. 3G), suggesting that
244 PDGFRα signaling influences Srsf3 binding specificity.

245

246 *Srsf3 and PDGFRα signaling are associated with differential GC content and length of*

247 *alternatively-spliced exons*

248 We next probed our RNA-seq dataset to determine whether specific transcript features

249 were associated with Srsf3-dependent AS. When comparing significant AS events between

250 scramble and shSrsf3 samples in the absence of PDGF-AA stimulation, we found that included

251 exons had a significantly higher GC content (median value of 53.4%) than both skipped exons

252 (50.0%) and exons that were not differentially alternatively spliced (51.2%) when Srsf3 is

253 present (Fig. 4A, Table S10). Additionally, we observed that included exons had a significantly

254 lower ratio of downstream intron to exon GC content (0.856) than both skipped exons (0.901)

255 and exons that were not differentially alternatively spliced (0.888) in the presence of Srsf3 (Fig.

256 4B, Table S10). The same comparisons revealed that the ratio of upstream and downstream

257 intron to exon length was significantly decreased in included exons (median values of 12.4 and

258 10.6, respectively) as compared to both skipped exons (19.5 and 20.0) and exons that were not

259 differentially alternatively spliced (14.2 and 13.3) in the presence of Srsf3 (Fig. 4C,D, Table

260 S10). Taken together, our data demonstrate that exons which are included in the presence of

261 Srsf3 tend to have a higher GC content and lower intron to exon length ratio.

262 To determine whether PDGFRα signaling had an effect on the transcript features to

263 which Srsf3 bound, we subsequently examined our eCLIP dataset. We found that the exon GC

264 content was significantly increased in exons bound by Srsf3 in the absence of ligand treatment

265 (median value of 57.9%) as compared to unbound exons (51.5%) (Fig. 4E, Table S10).

266 However, exon GC content was similar between unbound exons and those bound by Srsf3

267 upon PDGF-AA stimulation (53.8%) (Fig. 4E, Table S10). These findings indicate that

268 PDGFRα signaling mediates binding of Srsf3 to exons with a lower GC content.

269

270 *Transcripts bound by Srsf3 that undergo alternative splicing upon PDGFRα signaling encode*
271 *regulators of PI3K signaling*
272 To determine which transcripts are directly bound by Srsf3 and subject to DE and/or AS,
273 we cross-referenced the eCLIP and RNA-seq datasets. We collated transcripts with an Srsf3
274 eCLIP peak that were uniquely detected in the -PDGF-AA or +PDGF-AA samples (2,660
275 transcripts across 3,388 peaks) (Tables S8 and S11). Similarly, we gathered differentially-
276 expressed genes (596) or differentially alternatively-spliced transcripts (985) uniquely found in
277 one of the four treatment comparisons (Fig. 5A, Table S11). Only 32 (5.4%) of the DE genes
278 were directly bound by Srsf3, while 233 (23.7%) of the alternatively-spliced transcripts had an
279 Srsf3 eCLIP peak, with very little overlap (1 transcript) between all three categories (Fig. 5A).
280 We next correlated the eCLIP peaks with AS events across all four treatment
281 comparisons by identifying transcripts in which Srsf3 bound within an alternatively-spliced exon
282 or within 250 bp of the neighboring introns (Tables S12-S15). In agreement with our findings
283 above for the entire eCLIP dataset, Srsf3 exhibited differential binding in exons and surrounding
284 the 5' and 3' splice sites upon PDGF-AA stimulation (Fig. S5A,B). We performed an unbiased
285 motif enrichment analysis of Srsf3 peaks within the overlapping datasets, again revealing
286 different motifs between ligand treatment conditions and an enrichment of GA-rich motifs in the
287 +PDGF-AA samples (Fig. S5C,D).
288 To determine whether transcripts that are differentially bound by Srsf3 and undergo
289 differential AS downstream of PDGFRα signaling contribute to shared biological outputs, we
290 conducted GO analysis of the 149 unique transcripts from the overlapping datasets. The most
291 significant terms for biological process involved protein phosphorylation and deacetylation, and
292 RNA metabolism (Fig. 5B). Given that PI3K-mediated PDGFRα signaling is critical for
293 craniofacial development and regulates AS in this context (Dennison et al., 2021; Fantauzzo &
294 Soriano, 2014; Klinghoffer et al., 2002), we turned our focus toward GO terms associated with

295 this signaling pathway. We noted enrichment of PI3K-related GO terms (Fig. 5C), which
296 encompassed the genes *Becn1, Wdr81* and *Acap3* (Fig. 5D). Related to their roles in PI3K
297 signaling, each of these gene products has been shown to regulate membrane and/or endocytic
298 trafficking. Phosphatidylinositol 3-phosphate (PI(3)P) is a critical component of early endosomes
299 and is mainly generated by conversion of phosphatidylinositol (PI) by the class III PI3K complex,
300 which includes Beclin-1 (encoded by *Becn1*) (Wallroth & Haucke, 2018). WDR81 and Beclin-1
301 have been shown to interact, resulting in decreased endosomal PI(3)P synthesis, PI(3)P
302 turnover and early endosome conversion to late endosomes (Liu et al., 2016). Importantly, this
303 role of WDR81 contributes to RTK degradation (Rapiteanu et al., 2016).
304 Within our data, Srsf3 binding was increased in *Becn1* exon 7 upon PDGF-AA
305 stimulation, at an enriched motif within the overlapping datasets, and we observed a
306 corresponding increase in retention of adjacent intron 7 (Fig. 5D,E). As *Becn1* intron 7 contains
307 a premature termination codon (PTC), this event is predicted to result in nonsense-mediated
308 decay (NMD) in the absence of Srsf3 (Fig. 5E). Srsf3 binding was also increased in *Wdr81* exon
309 8 in response to PDGF-AA treatment, and our analyses revealed a corresponding increase in
310 excision of adjacent exon 9 (Fig. 5D,E). Because *Wdr81* exon 9 encodes two WD-repeat
311 domains, which are generally believed to form a β propellor structure required for protein
312 interactions (Li & Roberts, 2001), this AS event is predicted to result in a protein missing a
313 functional domain (Fig. 5E). These splicing patterns predict increased levels of Beclin-1 and
314 decreased levels of functional Wdr81 in the presence of Srsf3 and PDGF-AA stimulation,
315 resulting in augmented early endosome formation.
316
317 *Srsf3 regulates early endosome size and phosphorylation of Akt downstream of PDGFRα*
318 *signaling*
319 Given that Srsf3 differentially binds to transcripts that encode proteins involved in early
320 endosomal trafficking downstream of PDGFRα signaling, we first examined the formation of

321 Rab5-positive early endosomes (Zerial & McBride, 2001) in response to a time course of PDGF-
322 AA ligand stimulation in scramble versus shSrsf3 cells. As expected, Rab5 puncta size
323 increased from 0 min ($9.79 \times 10^{-4} \pm 1.13 \times 10^{-4}$ arbitrary units; mean ± s.e.m.) to 15 min of ligand
324 stimulation ($2.01 \times 10^{-3} \pm 7.20 \times 10^{-4}$ arbitrary units) in scramble cells, and significantly so by 60
325 min ($2.58 \times 10^{-3} \pm 9.20 \times 10^{-4}$ arbitrary units) (Fig. 6A, C-C", E-E", G-G"). However, this increase
326 was not observed in the absence of Srsf3 ($9.21 \times 10^{-4} \pm 1.61 \times 10^{-4}$ arbitrary units at 60 min)
327 (Fig. 6A, D-D", F-F", H-H"), demonstrating that Srsf3-mediated PDGFRα signaling leads to
328 enlarged early endosomes.

329 We next examined colocalization of PDGFRα with Rab5, as an estimate of receptor
330 levels in the early endosome. Colocalization levels increased from 0 min (0.332 ± 0.0832
331 Pearson's correlation coefficient (PCC); mean ± s.e.m.) to 15 min (0.429 ± 0.108 PCC) of
332 PDGF-AA treatment in scramble cells, then decreased to near baseline levels by 60 min (0.348
333 ± 0.0885 PCC) (Fig. 6B, C-C", E-E", G-G") as a subset of PDGFRα homodimers are likely
334 trafficked to late endosomes (Rogers et al., 2022). Strikingly, shSrsf3 cells exhibited a
335 significant decrease in colocalization between PDGFRα and Rab5 by 60 min of ligand treatment
336 (0.186 ± 0.0102 PCC) (Fig. 6B, D-D", F-F", H-H"), indicating that Srsf3 activity downstream of
337 PDGFRα signaling results in retention of PDGFRα in early endosomes.

338 Finally, we previously demonstrated that rapid internalization of PDGFRα homodimers
339 following PDGF-AA ligand stimulation is critical for downstream AKT phosphorylation (Rogers et
340 al., 2022). As such, we examined phospho-Akt levels as a readout of PDGFRα activation in
341 early endosomes. While PDGF-AA treatment for 15 min induced a robust phospho-Akt
342 response in scramble cells (13.5 ± 7.39 relative induction, mean ± s.e.m.) this response was
343 muted in shSrsf3 cells at the same timepoint (5.73 ± 1.91) (Fig. 6I). These findings further
344 suggest that retention of PDGFRα in early endosomes leads to increases in downstream PI3K-
345 mediated Akt signaling. Collectively, our data point to a feedback loop in which PI3K/Akt-

346 mediated PDGFRα signaling results in the nuclear translocation of Srsf3 and the subsequent
347 AS of transcripts to decrease levels of proteins that promote PDGFRα trafficking out of early
348 endosomes (Fig. 6J).
349
350 **Discussion**
351 In this study, we confirmed our prior *in vivo* results in the mouse embryonic facial
352 mesenchyme (Dennison et al., 2021) that PDGFRα signaling primary regulates gene expression
353 via AS. PDGF-AA-dependent differential gene expression was minimal following one hour of
354 ligand treatment and led to increased expression of immediate early genes *Klf10, Egf3* and
355 *Egr1*, consistent with previous findings (Vasudevan et al., 2015) and in line with the enriched
356 GO terms of regulation of transcription and DNA binding. Alternatively, PDGF-AA-dependent
357 alternatively-spliced transcripts were enriched for protein kinase activity, consistent with our
358 prior AS findings upon disruption of PI3K-mediated PDGFRα signaling in the palatal shelf
359 mesenchyme (Dennison et al., 2021). Importantly, our results demonstrated a significant
360 dependence on the RBP Srsf3 for AS downstream of PDGFRα activation. In fact, we found that
361 79% of Srsf3-dependent and 97% of PDGF-AA-dependent alternatively-spliced transcripts were
362 responsive to both Srsf3 activity and PDGFRα signaling. As discussed above, Srsf3 is
363 phosphorylated downstream of multiple stimuli (Bavelloni et al., 2014; Dennison et al., 2021;
364 Fantauzzo & Soriano, 2014; Long et al., 2019; Zhou et al., 2012), and it is likely that these
365 additional inputs contributed to Srsf3-dependent AS that was non-responsive to PDGF-AA
366 treatment. Further, our previous mass spectrometry screen identified 11 additional RBPs
367 involved in AS that are phosphorylated by Akt downstream of PI3K-mediated PDGFRα signaling
368 in primary MEPM cells (Fantauzzo & Soriano, 2014), which may account for the small fraction of
369 PDGF-AA-dependent AS that was non-responsive to Srsf3 knockdown. However, our RNA-seq
370 results together with the phenotypic overlap of embryos with neural crest-specific ablation of

371 *Srsf3* and mutant mouse models of *Pdgfra* and/or its ligands (Andrae et al., 2016; Dennison et
372 al., 2021; Ding et al., 2004; Fantauzzo & Soriano, 2014; Fredriksson et al., 2012; Klinghoffer et
373 al., 2002; Soriano, 1997) make a compelling case for Srsf3 serving as a critical effector of
374 PDGFRα signaling in the facial mesenchyme.

375 Here, we observed that Srsf3-dependent skipped exon events were enriched for
376 transcripts with a +ΔPSI (exon skipped more often in shSrsf3 samples) in the absence of PDGF-
377 AA stimulation, consistent with Srsf3 promoting exon inclusion. Alternatively, PDGF-AA ligand
378 treatment led to an increase in the percentage of Srsf3-dependent transcripts with a -ΔPSI
379 (exon included more often in shSrsf3 samples), suggesting that PDGFRα signaling causes
380 decreased exon inclusion in the presence of Srsf3. Interestingly, a recent paper found that
381 tethering Srsf3 downstream of the 5' splice site or upstream of the 3' splice site using MS2 stem
382 loops did not lead to AS of a splicing reporter (Schmok et al., 2024). However, the assay did not
383 test tethering within the exon and used a single minigene sequence context, and thus had the
384 potential to lead to false negative results (Schmok et al., 2024). Whether phosphorylation of
385 Srsf3 directly influences its binding to target RNAs or acts to modulate Srsf3 protein-protein
386 interactions which then contribute to differential RNA binding remains to be determined, though
387 findings from Schmok et al., 2024 may argue for the latter mechanism. Studies identifying
388 proteins that differentially interact with Srsf3 in response to PDGF-AA ligand stimulation are
389 ongoing and will shed light on these mechanisms.

390 This study represents the first endogenous CLIP analysis of Srsf3 in the absence of
391 protein tagging, and thus circumvents potential limitations with prior approaches in which
392 assayed RBPs were overexpressed and/or fused to another protein. Our eCLIP analyses
393 revealed several changes in Srsf3 transcript binding downstream of PDGF-AA stimulation,
394 including increased Srsf3 binding to exons and loss of Srsf3 binding to canonical CA-rich motifs.
395 A previous CLIP study using a stably integrated SRSF3-EGFP transgene in mouse P19 cells

396 determined that SRSF3 binding was enriched in exons, particularly within 100 nucleotides of the
397 5' and, to a lesser extent, 3' splice sites (Änkö et al., 2012), consistent with our results. This
398 same study identified a CA-rich canonical SRSF3 motif (Änkö et al., 2012). While such motifs
399 were identified here in the absence of PDGF-AA treatment, they were lost upon ligand
400 stimulation. Again, this shift could be due to loss of RNA binding owing to electrostatic repulsion
401 and/or changes in ribonucleoprotein composition and will be the subject of future studies.
402 Our findings additionally pointed to novel properties of exons whose inclusion is
403 dependent on Srsf3 in the absence of PDGFRα signaling. We demonstrated that these included
404 exons had a higher GC content, a lower ratio of downstream intron to exon GC content and a
405 decreased ratio of upstream and downstream intron to exon length. These findings are
406 consistent with previous results demonstrating that included exons tend to have higher GC
407 content than the flanking introns (Amit et al., 2012). Of note, PDGF-AA ligand stimulation
408 resulted in binding of Srsf3 to exons with a lower GC content, again suggesting that
409 phosphorylation of the RBP downstream of this signaling axis promotes exon skipping.
410 By cross-referencing our RNA-seq and eCLIP datasets, we showed that 24% of the
411 alternatively-spliced transcripts across our four treatment comparisons had an Srsf3 eCLIP
412 peak. As Srsf3 also has functions in the cytoplasm, such as RNA trafficking, translation and
413 degradation (Howard & Sanford, 2015), the additional eCLIP peaks may reflect alternate roles
414 for Srsf3 in RNA metabolism. Conversely, Srsf3-mediated AS may be delayed following
415 transcript binding in the short timeframe of our experimental design. However, the extent of
416 overlap that we observed is in line with previous studies correlating alternatively-spliced
417 transcripts upon knockdown of an RBP with endogenous eCLIP results for that same RBP,
418 including Rbfox2 (10%) (Moss et al., 2023) and LUC7L2 (18-26%) (Jourdain et al., 2021). The
419 degree to which our RNA-seq and eCLIP datasets overlapped here points to the robustness and
420 biological significance of our findings.

421 Our combined analyses demonstrated that Srsf3 binds and mediates the AS of
422 transcripts that encode proteins that regulate PI3K signaling and early endosomal trafficking
423 downstream of PDGFRα activation, including *Becn1, Wdr81* and *Acap3.* Homozygous missense
424 mutations in *WDR81* cause Cerebellar ataxia, impaired intellectual development, and
425 dysequilibrium syndrome 2 (OMIM 610185) in humans (Gulsuner et al., 2011), with some
426 patients exhibiting coarse facial features and strabismus (Garcias & Roth, 2007), pointing to a
427 critical role for this gene product in craniofacial development. Consistently, we found that related
428 GO terms, such as phosphatidylinositol phosphate binding and endosome to lysosome
429 transport, were significantly enriched among alternatively-spliced transcripts in murine
430 embryonic facial mesenchyme upon loss of PI3K binding to PDGFRα and/or knockdown of
431 *Srsf3* (Dennison et al., 2021). These data further confirm that our iMEPM model system served
432 as a powerful platform to uncover mechanisms that are utilized during craniofacial development
433 *in vivo*.
434 Our subsequent *in vitro* validation studies showed that Srsf3-mediated PDGFRα
435 signaling results in enlarged early endosomes, retention of the receptor in these early
436 endosomes and increased downstream PI3K-mediated Akt signaling. Relatedly, we and others
437 have linked spatial organization with the propagation of PDGFRα signaling, such that rapid
438 internalization of the receptors into early endosomes or autophagy of the receptors are required
439 for maximal phosphorylation of AKT downstream of PDGFRα activation (Rogers et al., 2022;
440 Simpson et al., 2024). Together, these results indicate a feedback loop at play in the
441 craniofacial mesenchyme in which stimulation of PDGFRα homodimer signaling leads to Srsf3-
442 dependent AS of transcripts, a subsequent increase in the levels of proteins that maintain the
443 receptor in early endosomes and a corresponding decrease in the levels of proteins that
444 promote trafficking of the receptor to late endosomes for eventual degradation. These findings
445 thus represent a novel mechanism by which PDGFRα activity is maintained and propagated

446 within the cell. Whether similar mechanisms exist downstream of alternate RTKs or contribute to
447 increases in the phosphorylation of effector proteins other than Akt remain to be determined.
448 Taken together, our findings significantly enhance our understanding of the molecular
449 mechanisms by which Srsf3 activity is regulated downstream of growth factor stimulation.
450 Interestingly, a recent study demonstrated that retention of another shuttling SR protein, Srsf1,
451 exclusively in the nucleus resulted in widespread ciliary defects in mice (Haward et al., 2021).
452 This finding indicates that dissecting nuclear from cytoplasmic functions of SR proteins can
453 provide powerful insight into the physiological relevance of each. Going forward, it will be critical
454 to explore the *in vivo* consequences of abrogating Akt-mediated phosphorylation of Srsf3 and
455 comparing the resulting phenotype to those of embryos with constitutive or conditional ablation
456 of *Srsf3* in the neural crest lineage (Dennison et al., 2021; Jumaa et al., 1999). These
457 experiments are ongoing and should shed considerable light on the roles of RBP post-
458 translational modifications during development.
459

460 **Materials and Methods**

461 *Generation of scramble and* Srsf3 *shRNA iMEPM cell lines*

462 Immortalized mouse embryonic palatal mesenchyme (iMEPM) cells were derived from a
463 male *Cdkn2a*$^{-/-}$ embryo as previously described (Fantauzzo & Soriano, 2017). iMEPM cells were
464 cultured in growth medium [Dulbecco's modified Eagle's medium (Gibco, Thermo Fisher
465 Scientific, Waltham, MA, USA) supplemented with 50 U/mL penicillin (Gibco), 50 μg/mL
466 streptomycin (Gibco) and 2 mM L-glutamine (Gibco) containing 10% fetal bovine serum (FBS)
467 (Hyclone Laboratories Inc., Logan, UT, USA)] and grown at 37°C in 5% carbon dioxide. iMEPM
468 cells were tested for mycoplasma contamination using the MycoAlert Mycoplasma Detection Kit
469 (Lonza Group Ltd, Basel, Switzerland). Packaged lentiviruses containing pLV[shRNA]-
470 EGFP:T2A:Puro-U6>Scramble_shRNA (vectorID: VB010000-0009mxc) with sequence

471 CCTAAGGTTAAGTCGCCCTCGCTCGAGCGAGGGCGACTTAACCTTAGG or pLV[shRNA]-
472 EGFP:T2A:Puro-U6>mSrsf3[shRNA#1] (vectorID: VB900060-7699yyh) with sequence
473 GAATGATAAAGCGGTGTTTACTCGAGTAAACACCGCTTTATCATTCC were purchased from
474 VectorBuilder (Chicago, IL, USA). Medium containing lentivirus for a multiplicity of infection of
475 10 for 200,000 cells with the addition of 10 ug/mL polybrene was added to iMEPM cells for 16 h,
476 and cells were subsequently grown in the presence of 4 ug/mL puromycin for 10 days. Cells
477 with the highest GFP expression (top 20%) were isolated on a Moflo XDP 100 cell sorter
478 (Beckman Coulter Inc., Brea, CA, USA) and expanded. Srsf3 expression in scramble and *Srsf3*
479 shRNA cell lines was confirmed by western blotting. Once the stable cell lines were established,
480 they were split at a ratio of 1:4 for maintenance. Scramble and *Srsf3* shRNA cells were used for
481 experiments at passages 9-20.
482
483 *Immunoprecipitation and western blotting*
484 To induce PDGFRα signaling, cells at ~70% confluence were serum starved for 24 h in
485 starvation medium [Dulbecco's modified Eagle's medium (Gibco) supplemented with 50 U/mL
486 penicillin (Gibco), 50 μg/mL streptomycin (Gibco) and 2 mM L-glutamine (Gibco) containing
487 0.1% FBS (Hyclone Laboratories Inc.)] and stimulated with 10 ng/mL rat PDGF-AA ligand (R&D
488 Systems, Minneapolis, MN, USA) diluted from a 1.5 μg/mL working solution in 40 nM HCl
489 containing 0.1% BSA for the indicated length of time. When applicable, UV-crosslinking was
490 performed at 254 nm and 400 mJ/cm^2 using a Vari-X-Link system (UVO3 Ltd, Cambridgeshire,
491 UK). For immunoprecipitation of Srsf3, cells were resuspended in ice-cold CLIP lysis buffer [50
492 mM Tris-HCl pH 7.4, 100 mM NaCl, 1% NP-40, 0.1% SDS, 0.5% sodium deoxycholate, 1x
493 complete Mini protease inhibitor cocktail (Roche, MilliporeSigma, Burlington, MA, USA), 1 mM
494 PMSF, 10 mM NaF, 1 mM Na_3VO_4, 25 mM β-glycerophosphate]. Cleared lysates were collected
495 by centrifugation at 18,000 *g* for 20 min at 4°C. Anti-Srsf3 antibody (10 μg/sample) (ab73891,

496 Abcam, Waltham, MA, USA) was added to protein A Dynabeads (125 μL/sample) (Thermo
497 Fisher Scientific) washed twice in ice-cold CLIP lysis buffer and incubated for 45 min at room
498 temperature. Cells lysates were incubated with antibody-conjugated Dynabeads or Dynabeads
499 M-280 sheep anti-rabbit IgG (Thermo Fisher Scientific) washed twice in ice-cold CLIP lysis
500 buffer overnight at 4°C. The following day, Dynabeads were washed twice each with ice-cold
501 high salt wash buffer [50 mM Tris-HCl pH 7.4, 1M NaCl, 1 mM EDTA, 1% NP-40, 0.1% SDS,
502 0.5% sodium deoxycholate] followed by ice-cold wash buffer [20 mM Tris-HCl pH 7.4, 10 mM
503 $MgCl_2$, 0.2% Tween-20]. The precipitated proteins were eluted with 1x NuPAGE LDS buffer
504 (Thermo Fisher Scientific) containing 100 mM dithiothreitol, heated for 10 minutes at 70°C, and
505 separated by SDS-PAGE. For western blotting of whole-cell lysates, protein lysates were
506 generated by resuspending cells in ice-cold NP-40 lysis buffer (20 mM Tris-HCl pH 8, 150 mM
507 NaCl, 10% glycerol, 1% Nonidet P-40, 2 mM EDTA, 1x complete Mini protease inhibitor cocktail
508 (Roche), 1 mM PMSM, 10 mM NaF, 1 mM Na_3VO_4, 25 mM β-glycerophosphate) and collecting
509 cleared lysates by centrifugation at 13,400 *g* at 4°C for 20 min. Laemmli buffer containing 10%
510 β-mercaptoethanol was added to the lysates, which were heated for 5 min at 100°C. Proteins
511 were subsequently separated by SDS-PAGE. Western blot analysis was performed according to
512 standard protocols using horseradish peroxidase-conjugated secondary antibodies. Blots were
513 imaged using a ChemiDoc XRS+ (Bio-Rad Laboratories, Inc., Hercules, CA, USA) or a
514 ChemiDoc (Bio-Rad Laboratories, Inc.). The following primary antibodies were used for western
515 blotting: Srsf3 (1:1,000, ab73891, Abcam), Gapdh (1:50,000, 60004, Proteintech Group, Inc.,
516 Rosemont, IL, USA), phospho-Akt (Ser473) (1:1,000, 9271, Cell Signaling Technology, Inc.,
517 Danvers, MA, USA), Akt (1:1,000, 9272, Cell Signaling Technology, Inc.), horseradish
518 peroxidase-conjugated goat anti-mouse IgG (1:20,000, 115035003, Jackson ImmunoResearch
519 Inc., West Grove, PA, USA), horseradish peroxidase-conjugated goat anti-rabbit IgG (1:20,000,
520 111035003;, Jackson ImmunoResearch Inc.). Quantifications of signal intensity were performed
521 with ImageJ software (version 1.53t, National Institutes of Health, Bethesda, MD, USA). Relative

522 phospho-Akt levels were determined by normalizing to total Akt levels. When applicable,
523 statistical analyses were performed with Prism 10 (GraphPad Software Inc., San Diego, CA,
524 USA) using a two-tailed, ratio paired *t*-test within each cell line and a two-tailed, unpaired *t*-test
525 with Welch's correction between each cell line. Immunoprecipitation and western blotting
526 experiments were performed across three independent experiments.
527
528 *RNA-sequencing and related bioinformatics analyses*
529 8×10^5 cells obtained from each of three independent biological replicates per treatment
530 were frozen on liquid nitrogen and stored at -80°C. Following thawing, total RNA was
531 simultaneously isolated from all samples using the RNeasy Mini Kit (Qiagen, Inc., Germantown,
532 MD, USA) according to the manufacturer's instructions. RNA was forwarded to the University of
533 Colorado Cancer Center Genomics Shared Resource for quality control, library preparation, and
534 sequencing. RNA purity, quantity and integrity were assessed with a NanoDrop (Thermo Fisher
535 Scientific) and a 4200 TapeStation System (Agilent Technologies, Inc., Santa Clara, CA, USA)
536 prior to library preparation. Total RNA (200 ng) was used for input into the Universal Plus
537 mRNA-Seq kit with NuQuant (Tecan Group Ltd., Männedorf, Switzerland). Dual index, stranded
538 libraries were prepared and sequenced on a NovaSeq 6000 Sequencing System (Illumina, San
539 Diego, CA, USA) to an average depth of ~54 million read pairs (2x150 bp reads).
540 Raw sequencing reads were de-multiplexed using bcl2fastq (Illumina). Trimming, filtering
541 and adapter contamination removal was performed using BBDuk (from the BBmap v35.85 tool
542 suite) (Bushnell, 2015). For differential expression analysis, transcript abundance was quantified
543 using Salmon (v1.4.0) (Patro et al., 2017) and a decoy-aware transcriptome index prepared
544 using GENCODE (Frankish et al., 2019) GRCm39 M26. Gene level summaries were calculated
545 using tximport (Soneson et al., 2016) in R and differential expression was measured using
546 DESeq2 (v.1.32.0) (Love et al., 2014). Significant changes in gene-level expression are
547 reported for cases with adjusted $P \leq 0.05$ and fold change $|FC| \geq 2$. Spearman correlation was

548 computed between conditions for differentially-expressed genes. For alternative splicing
549 analysis, raw FASTQ were trimmed to a uniform length of 125 bp. Reads were aligned to the
550 mouse genome (GRCm39 Gencode M26) using STAR (v.2.7.9a) (Dobin et al., 2013). Additional
551 parameters for STAR: --outFilterType BySJout --outFilterMismatchNmax 10 --
552 outFilterMismatchNoverLmax 0.04 --alignEndsType EndToEnd --runThreadN 16 --
553 alignSJDBoverhangMin 4 --alignIntronMax 300000 --alignSJoverhangMin 8 --alignIntronMin 20.
554 All splice junctions detected in at least 1 read from the first pass alignment were used in a
555 second pass alignment, per software documentation. Alternative splicing events were detected
556 using rMATS (v4.0.2, default parameters plus '—cstat 0.0001') (Shen et al. 2014). Reads
557 mapping to the splice junction as well as those mapping to the exon body were used in
558 downstream analyses. Detected events were compared between treatment groups and
559 considered significant with false discovery rate (FDR) ≤ 0.05, a difference in percent spliced in
560 ($|\Delta PSI|$) ≥ 0.05 and event detection in at least 10 reads in either condition. Raw read pairs,
561 trimmed read pairs for Salmon input, Salmon mapping rate per sample, trimmed read pairs (125
562 bp) for STAR input and STAR unique mapping rate can be found in Table S1. Gene ontology
563 analysis was performed with various libraries from the Enrichr gene list enrichment analysis tool
564 (Chen et al., 2013; Kuleshov et al., 2016) and terms with $P < 0.05$ were considered significant.
565
566 *qPCR*
567 Total RNA was isolated using the RNeasy mini kit (Qiagen, Germantown, MD, USA)
568 according to the manufacturer's instructions. First-strand cDNA was synthesized using a ratio of
569 2:1 random primers:oligo (dT) primer and SuperScript II RT (Invitrogen, Thermo Fisher
570 Scientific) according to the manufacturer's instructions. All reactions were performed with 1×
571 ThermoPol buffer [0.02 M Tris (pH 8.8), 0.01 M KCl, 0.01 M $(NH_4)_2SO_4$, 2 mM $MgSO_4$ and 0.1%
572 Triton X-100], 200 μM dNTPs, 200 nM primers (Integrated DNA Technologies, Inc., Coralville,

573 IA, USA), 0.6 U Taq polymerase and 1 µg cDNA in a 25 µL reaction volume. The primers used
574 can be found in Table S16. The following PCR protocol was used for *Arhgap12*: step1, 3 min at
575 94°C; step 2, 30 s at 94°C; step 3, 30 s at 47°C; step 4, 30 s at 72°C; repeat steps 2-4 for 34
576 cycles; and step 5, 5 min at 72°C. The following PCR protocol was used for *Cep55*: step1, 3 min
577 at 94°C; step 2, 30 s at 94°C; step 3, 30 s at 48°C; step 4, 30 s at 72°C; repeat steps 2-4 for 34
578 cycles; and step 5, 5 min at 72°C. Two-thirds of total PCR products were electrophoresed on a
579 2% agarose/TBE gel containing ethidium bromide and photographed on an Aplegen Omega
580 Fluor Gel Documentation System (Aplegen Inc., Pleasanton, CA, USA). Quantifications of band
581 intensity were performed with ImageJ software (version 1.53t, National Institutes of Health). The
582 PSI was calculated independently for each sample as the percentage of the larger isoform
583 divided by the total abundance of all isoforms within the given gel lane. Statistical analyses were
584 performed with Prism 10 (GraphPad Software) using a two-tailed, unpaired *t*-test with Welch's
585 correction. qPCR reactions were performed using three biological replicates.
586
587 *Enhanced UV-crosslinking and immunoprecipitation and related bioinformatics analyses*
588 Experiments were performed as previously described in biological duplicates (Van
589 Nostrand et al., 2016, 2017). Briefly, 2 million cells per treatment were serum starved and
590 treated with 10 ng/mL PDGF-AA as described above. Cells were subsequently UV-crosslinked
591 at 254 nm and 400 mJ/cm^2, scraped in 1x phosphate buffered saline (PBS) and transferred to
592 1.5 mL Eppendorf tubes, at which point excess PBS was removed and cells were frozen on
593 liquid nitrogen and stored at -80°C. Following thawing, cells were lysed in ice-cold CLIP lysis
594 buffer, sonicated by BioRuptor (Diagenode, Denville, NJ, USA) and treated with RNase I
595 (Thermo Fisher Scientific). 2% of lysates were set aside as size-matched input samples. Srsf3-
596 RNA complexes were immunoprecipitated with anti-Srsf3 antibody (10 µg per sample)
597 (ab73891, Abcam) conjugated to protein A Dynabeads (Thermo Fisher Scientific). IP samples
598 were washed and dephosphorylated with FastAP (New England Biolabs, Ipswich, MA, USA)

599 and T4 PNK (New England Biolabs). IP samples underwent on-bead ligation of barcoded RNA
600 adapters (/5phos/rArGrArUrCrGrGrArArGrArGrCrGrUrCrGrUrG/3SpC3/) to the 3' end using T4
601 RNA ligase (New England Biolabs). Following elution, protein-RNA complexes were run on 4-
602 12% Bis-Tris 1.5 mm gels (Thermo Fisher Scientific) and transferred onto nitrocellulose
603 membranes. The 20-75 kDa region was excised and digested with proteinase K (New England
604 Biolabs). RNA was isolated with acid phenol/chloroform/isoamyl alcohol (pH 6.5) (Thermo
605 Fisher Scientific), reverse transcribed with Superscript III (Thermo Fisher Scientific) and treated
606 with ExoSAP-IT (Affymetrix, Thermo Fisher Scientific) to remove excess primers and
607 unincorporated nucleotides. Samples underwent 3' ligation of barcoded DNA adapters
608 (/5Phos/NNNNNNNNNNAGATCGGAAGAGCACACGTCTG/3SpC3/), clean-up with Dynabeads
609 MyOne Silane (Thermo Fisher Scientific) and qPCR to determine the appropriate number of
610 PCR cycles. Libraries were then amplified with Q5 PCR mix (New England Biolabs) for a total of
611 16-25 cycles. Libraries were forwarded to the University of Colorado Cancer Center Genomics
612 Shared Resource for quality control and sequencing. Sample integrity was assessed with a
613 D1000 ScreenTape System (Agilent Technologies, Inc.) and sequenced on a NovaSeq 6000
614 Sequencing System (Illumina) to an average depth of ~20 million read pairs (2x150 bp reads).
615 Raw sequencing reads were de-multiplexed using bcl2fastq (Illumina). Adapters were
616 trimmed using cutadapt (v.1.18) (Martin, 2011). Trimmed reads were quality filtered and
617 collapsed using a combination of FASTX-Toolkit (v.0.0.14)
618 (http://hannonlab.cshl.edu/fastx_toolkit), seqtk (v.1.3-r106) (https://github.com/lh3/seqtk) and
619 custom scripts. After collapsing the reads, unique molecular identifiers were removed using
620 seqtk. STAR index for repetitive elements was created using repetitive sequences from
621 msRepDB (Liao et al., 2022). Reads ≥ 18 nt were mapped to the repetitive elements using
622 STAR (v.2.7.9a) (Dobin et al. 2013). Reads unmapped to the repetitive elements were mapped
623 to the mouse genome (GRCm39 Gencode M26) using STAR (v.2.7.9a) with parameters
624 alignEndsType: EndtoEnd and outFilterMismatchNoverReadLmax: 0.04. Peaks were called

625 using omniCLIP (v.0.20) (Drewe-Boss et al., 2018) with the foreground penalty (--fg_pen)
626 parameter set to 5. Peaks were annotated and motif analyses performed using RCAS (v.1.19.0)
627 (Uyar et al., 2017) and custom R script. For visualization purposes, bigWig files were created
628 from bam files using deepTools (v.3.5.5) (Ramírez et al., 2016). Peaks were visualized in
629 Integrative Genomics Viewer (v.2.13.0) (Robinson et al., 2011). Intron and exon features were
630 calculated using Matt (v.1.3.1) (Gohr & Irimia, 2019), and statistical analyses were performed
631 using a Mann-Whitney U test. For overlap of eCLIP peaks and alternative splicing events, peak
632 coordinates were taken from omniCLIP bed files and alternative splicing coordinates were taken
633 from rMATS output. Overlapping coordinates from alternative splicing events were defined
634 following the rMAPS default values (Park et al., 2016). Overlap was calculated using valr
635 (v.0.6.4) (Riemondy et al., 2017) and custom R scripts. Raw read pairs, trimmed read pairs,
636 collapsed reads, reads after removing repetitive elements, mapped reads, peaks and annotated
637 peaks can be found in Table S7. Gene ontology analysis was performed with various libraries
638 from the Enrichr gene list enrichment analysis tool (Chen et al., 2013; Kuleshov et al., 2016) and
639 terms with $P < 0.05$ were considered significant.
640
641 *Immunofluorescence analysis*
642 Cells were seeded onto glass coverslips at ~40% confluency per 24-well plate well in
643 iMEPM growth medium. After 24 h, cells were serum starved and treated with 10 ng/mL PDGF-
644 AA as described above. Cells were fixed in 4% paraformaldehyde (PFA) in PBS with 0.1%
645 Triton X-100 for 10 min and washed in PBS. Cells were blocked for 1 h in 5% normal donkey
646 serum (Jackson ImmunoResearch Inc.) in PBS and incubated overnight at 4°C in primary
647 antibody diluted in 1% normal donkey serum in PBS. After washing in PBS, cells were
648 incubated in Alexa Fluor 488-conjugated donkey anti-rabbit secondary antibody (1:1,000;
649 A21206; Invitrogen) or Alexa Fluor 546-conjugated donkey anti-mouse secondary antibody
650 (1:1,000; A10036; Invitrogen) diluted in 1% normal donkey serum in PBS with 2 µg/ml DAPI

651 (Sigma-Aldrich, St. Louis, MO, USA) for 1 h. Cells were mounted in VECTASHIELD HardSet
652 Antifade Mounting Medium (Vector Laboratories, Inc., Burlingame, CA, USA) and photographed
653 using an Axiocam 506 mono digital camera (Carl Zeiss Microscopy LLC, White Plains, NY,
654 USA) fitted onto an Axio Observer 7 fluorescence microscope (Carl Zeiss Microscopy LLC) with
655 the 63x oil objective with a numerical aperture of 1.4 at room temperature. The following
656 antibodies were used for immunofluorescence analysis: Rab5 (1:200, C8B1, 3547, Cell
657 Signaling Technology Inc.), PDGFRα (1:20, AF1062, R&D Systems). For assessment of Rab5
658 puncta size and colocalization experiments, three independent trials, or biological replicates,
659 were performed. For each biological replicate, 20 technical replicates consisting of individual
660 cells were imaged with Z-stacks (0.24 μm between Z-stacks with a range of 1–6 Z-stacks) per
661 timepoint. Images were deconvoluted using ZEN Blue software (Carl Zeiss Microscopy LLC)
662 using the 'Better, fast (Regularized Inverse Filter)' setting. Extended depth of focus was applied
663 to Z-stacks using ZEN Blue software (Carl Zeiss Microscopy LLC) to generate images with the
664 maximum depth of field. For assessment of Rab5 puncta size, images were converted to 8-bit
665 using Fiji software (version 2.14.0/1.54f). Images were subsequently converted to a mask and
666 watershed separation was applied. A region of interest (ROI) was drawn around each Rab5-
667 positive cell and particles were analyzed per cell using the "analyze particles" function. For
668 colocalization measurements, an ROI was drawn around each PDGFRα-positive cell in the
669 corresponding Cy3 (marker) channel using Fiji. For each image with a given ROI, the Cy3
670 channel and the EGFP channel were converted to 8-bit images. Colocalization was measured
671 using the Colocalization Threshold function, where the rcoloc value [Pearson's correlation
672 coefficient (PCC)] was used in statistical analysis. Statistical analyses were performed on the
673 average values from each biological replicate with Prism 10 (GraphPad Software Inc.) using a
674 two-way ANOVA followed by uncorrected Fisher's LSD test.
675

676 **Acknowledgements**

677 We are grateful to Jessica Johnston and Erin Binne for technical assistance, and Drs. Allison
678 Swain, Justin Roberts and Aaron Johnson at the University of Colorado Anschutz Medical
679 Campus for advice on eCLIP experiments. Cell sorting was performed at the University of
680 Colorado Cancer Center Flow Cytometry Shared Resource with assistance from Dr. Dmitry
681 Baturin. RNA-seq and eCLIP sequencing experiments were performed at University of Colorado
682 Cancer Center Genomics Shared Resource. We thank members of the Fantauzzo laboratory for
683 their critical comments on the manuscript.

684

685 **Competing Interests**

686 The authors declare no competing or financial interests.

687

688 **Author contributions**

689 Conceptualization: TEF, MS, NM, KAF; Methodology: TEF, MS, NM, KAF; Formal analysis:
690 TEF, MS, EDL, KAF; Investigation: TEF, MS, EDL; Writing – Original Draft: TEF, KAF; Writing –
691 Review & Editing: MS, EDL, NM; Visualization: TEF, MS, KAF; Supervision: NM, KAF; Project
692 administration: KAF; Funding acquisition: TEF, KAF.

693

694 **Funding**

695 This work was supported by National Institutes of Health grants R01DE030864 (to K.A.F.),
696 R35GM147025 (to N.M.), the University of Colorado Anschutz Medical Campus RNA
697 Bioscience Initiative (to N.M. and M.P.S.) and F31DE032252 (to T.E.F.). The Flow Cytometry
698 Shared Resource and Genomics Shared Resource are supported by National Institutes of
699 Health grant P30CA046934.

700

701 **Data Availability**

The eCLIP and RNA-sequencing datasets generated during this study have been deposited in GEO under SuperSeries accession number GSE263170. Custom analysis scripts will be provided by Dr. Larson through GitHub.

References

Akerman, M., David-Eden, H., Pinter, R. Y., & Mandel-Gutfreund, Y. (2009). A computational approach for genome-wide mapping of splicing factor binding sites. *Genome Biology*, *10*(3), R30. https://doi.org/10.1186/gb-2009-10-3-r30

Amit, M., Donyo, M., Hollander, D., Goren, A., Kim, E., Gelfman, S., Lev-Maor, G., Burstein, D., Schwartz, S., Postolsky, B., Pupko, T., & Ast, G. (2012). Differential GC Content between Exons and Introns Establishes Distinct Strategies of Splice-Site Recognition. *Cell Reports*, *1*(5), 543–556. https://doi.org/10.1016/j.celrep.2012.03.013

Andrae, J., Gouveia, L., Gallini, R., He, L., Fredriksson, L., Nilsson, I., Johansson, B. R., Eriksson, U., & Betsholtz, C. (2016). A role for PDGF-C/PDGFRα signaling in the formation of the meningeal basement membranes surrounding the cerebral cortex. *Biology Open*, *5*(4), 461–474. https://doi.org/10.1242/bio.017368

Änkö, M.-L., Müller-McNicoll, M., Brandl, H., Curk, T., Gorup, C., Henry, I., Ule, J., & Neugebauer, K. M. (2012). The RNA-binding landscapes of two SR proteins reveal unique functions and binding to diverse RNA classes. *Genome Biology*, *13*(3), R17. https://doi.org/10.1186/gb-2012-13-3-r17

Bavelloni, A., Piazzi, M., Faenza, I., Raffini, M., D'Angelo, A., Cattini, L., Cocco, L., & Blalock, W. L. (2014). Prohibitin 2 represents a novel nuclear AKT substrate during all- *trans* retinoic acid–induced differentiation of acute promyelocytic leukemia cells. *The FASEB Journal*, *28*(5), 2009–2019. https://doi.org/10.1096/fj.13-244368

Bebee, T. W., Park, J. W., Sheridan, K. I., Warzecha, C. C., Cieply, B. W., Rohacek, A. M., Xing, Y., & Carstens, R. P. (2015). The splicing regulators Esrp1 and Esrp2 direct an

728 epithelial splicing program essential for mammalian development. *eLife*, *4*, e08954.
729 https://doi.org/10.7554/eLife.08954
730 Bushnell, B. (2015). *BBMap*. Https://Sourceforge.Net/Projects/Bbmap/.
731 https://sourceforge.net/projects/bbmap/
732 Chen, E. Y., Tan, C. M., Kou, Y., Duan, Q., Wang, Z., Meirelles, G. V., Clark, N. R., & Ma'ayan,
733 A. (2013). Enrichr: Interactive and collaborative HTML5 gene list enrichment analysis
734 tool. *BMC Bioinformatics*, *14*, 128. https://doi.org/10.1186/1471-2105-14-128
735 Choi, S. J., Marazita, M. L., Hart, P. S., Sulima, P. P., Field, L. L., McHenry, T. G., Govil, M.,
736 Cooper, M. E., Letra, A., Menezes, R., Narayanan, S., Mansilla, M. A., Granjeiro, J. M.,
737 Vieira, A. R., Lidral, A. C., Murray, J. C., & Hart, T. C. (2009). The PDGF-C regulatory
738 region SNP rs28999109 decreases promoter transcriptional activity and is associated
739 with CL/P. *European Journal of Human Genetics*, *17*(6), 774–784.
740 https://doi.org/10.1038/ejhg.2008.245
741 Cibi, D. M., Mia, M. M., Guna Shekeran, S., Yun, L. S., Sandireddy, R., Gupta, P., Hota, M.,
742 Sun, L., Ghosh, S., & Singh, M. K. (2019). Neural crest-specific deletion of Rbfox2 in
743 mice leads to craniofacial abnormalities including cleft palate. *eLife*, *8*, e45418.
744 https://doi.org/10.7554/eLife.45418
745 Dennison, B. J. C., Larson, E. D., Fu, R., Mo, J., & Fantauzzo, K. A. (2021). Srsf3 mediates
746 alternative RNA splicing downstream of PDGFRα signaling in the facial mesenchyme.
747 *Development*, *148*(14), dev199448. https://doi.org/10.1242/dev.199448
748 Ding, H., Wu, X., Boström, H., Kim, I., Wong, N., Tsoi, B., O'Rourke, M., Koh, G. Y., Soriano, P.,
749 Betsholtz, C., Hart, T. C., Marazita, M. L., Field, L. L., Tam, P. P. L., & Nagy, A. (2004).
750 A specific requirement for PDGF-C in palate formation and PDGFR-α signaling. *Nature*
751 *Genetics*, *36*(10), 1111–1116. https://doi.org/10.1038/ng1415
752 Dobin, A., Davis, C. A., Schlesinger, F., Drenkow, J., Zaleski, C., Jha, S., Batut, P., Chaisson,

753 M., & Gingeras, T. R. (2013). STAR: ultrafast universal RNA-seq aligner. *Bioinformatics, 29*(1), 15-21. https://doi.org/10.1093/bioinformatics/bts635

755 Drewe-Boss, P., Wessels, H.-H., & Ohler, U. (2018). omniCLIP: Probabilistic identification of protein-RNA interactions from CLIP-seq data. *Genome Biology*, *19*(1), 183. https://doi.org/10.1186/s13059-018-1521-2

758 Fantauzzo, K. A., & Soriano, P. (2014). PI3K-mediated PDGFR signaling regulates survival and proliferation in skeletal development through p53-dependent intracellular pathways. *Genes & Development*, *28*(9), 1005–1017. https://doi.org/10.1101/gad.238709.114

761 Fantauzzo, K. A., & Soriano, P. (2017). Generation of an immortalized mouse embryonic palatal mesenchyme cell line. *PLOS ONE*, *12*(6), e0179078. https://doi.org/10.1371/journal.pone.0179078

764 Forman, T. E., Dennison, B. J. C., & Fantauzzo, K. A. (2021). The Role of RNA-Binding Proteins in Vertebrate Neural Crest and Craniofacial Development. *Journal of Developmental Biology*, 19.

767 Frankish, A., Diekhans, M., Ferreira, A. M., Johnson, R., Jungreis, I., Loveland, J., Mudge, J. M., Sisu, C., Wright, J., Armstrong, J., Barnes, I., Berry, A., Bignell, A., Carbonell Sala, S., Chrast, J., Cunningham, F., Di Domenico, T., Donaldson, S., Fiddes, I. T., … Flicek, P. (2019). GENCODE reference annotation for the human and mouse genomes. *Nucleic Acids Research*, *47*(D1), D766-763. https://doi.org/10.1093/nar/gky955

772 Fredriksson, L., Nilsson, I., Su, E. J., Andrae, J., Ding, H., Betsholtz, C., Eriksson, U., & Lawrence, D. A. (2012). Platelet-Derived Growth Factor C Deficiency in C57BL/6 Mice Leads to Abnormal Cerebral Vascularization, Loss of Neuroependymal Integrity, and Ventricular Abnormalities. *The American Journal of Pathology*, *180*(3), 1136–1144. https://doi.org/10.1016/j.ajpath.2011.12.006

777 Fu, X.-D., & Ares, M. (2014). Context-dependent control of alternative splicing by RNA-binding proteins. *Nature Reviews Genetics*, *15*(10), 689–701. https://doi.org/10.1038/nrg3778

Fu, X.-D., & Maniatis, T. (1990). Factor required for mammalian spliceosome assembly is localized to discrete regions in the nucleus. *Nature*, *343*(6257), 437–441. https://doi.org/10.1038/343437a0

Garcias, G. D. L., & Roth, M. D. G. M. (2007). A Brazilian family with quadrupedal gait, severe mental retardation, coarse facial characteristics, and hirsutism. *International Journal of Neuroscience*, *117*(7), 927–933. https://doi.org/10.1080/00207450600910721

Gohr, A., & Irimia, M. (2019). *Matt*: Unix tools for alternative splicing analysis. *Bioinformatics*, *35*(1), 130–132. https://doi.org/10.1093/bioinformatics/bty606

Gulsuner, S., Tekinay, A. B., Doerschner, K., Boyaci, H., Bilguvar, K., Unal, H., Ors, A., Onat, O. E., Atalar, E., Basak, A. N., Topaloglu, H., Kansu, T., Tan, M., Tan, U., Gunel, M., & Ozcelik, T. (2011). Homozygosity mapping and targeted genomic sequencing reveal the gene responsible for cerebellar hypoplasia and quadrupedal locomotion in a consanguineous kindred. *Genome Research*, *21*(12), 1995-2003. https://doi.org/10.1101/gr.126110.111.

Haward, F., Maslon, M. M., Yeyati, P. L., Bellora, N., Hansen, J. N., Aitken, S., Lawson, J., von Kriegsheim, A., Wachten, D., Mill, P., Adams, I. R., & Caceres, J. F. (2021). Nucleo-cytoplasmic shuttling of splicing factor SRSF1 is required for development and cilia function. *eLife*, *10*, e65104. https://doi.org/10.7554/eLife.65104

He, F., & Soriano, P. (2013). A critical role for PDGFRalpha signaling in medial nasal process development. *PLoS Genetics, 9*(9), e1003851. https://doi.org/10.1371/journal.pgen.1003851

Howard, J. M., & Sanford, J. R. (2015). The RNAissance family: SR proteins as multifaceted regulators of gene expression: *Wiley Interdisciplinary Reviews: RNA*, *6*(1), 93–110. https://doi.org/10.1002/wrna.1260

803 Huang, Y., Yario, T. A., & Steitz, J. A. (2004). A molecular link between SR protein
804 dephosphorylation and mRNA export. *Proceedings of the National Academy of*
805 *Sciences*, *101*(26), 9666–9670. https://doi.org/10.1073/pnas.0403533101
806 Jourdain, A. A., Begg, B. E., Mick, E., Shah, H., Calvo, S. E., Skinner, O. S., Sharma, R., Blue,
807 S. M., Yeo, G. W., Burge, C. B., & Mootha, V. K. (2021). Loss of LUC7L2 and U1 snRNP
808 subunits shifts energy metabolism from glycolysis to OXPHOS. *Molecular Cell*, *81*(9),
809 1905-1919.e12. https://doi.org/10.1016/j.molcel.2021.02.033
810 Jumaa, H., Wei, G., & Nielsen, P. J. (1999). Blastocyst formation is blocked in mouse embryos
811 lacking the splicing factor SRp20. *Current Biology*, *9*(16), 899–902.
812 https://doi.org/10.1016/S0960-9822(99)80394-7
813 Klinghoffer, R. A., Hamilton, T. G., Hoch, R., & Soriano, P. (2002). An Allelic Series at the
814 PDGFaR Locus Indicates Unequal Contributions of Distinct Signaling Pathways During
815 Development. *Developmental Cell*, *2*, 103–113.
816 Krainer, R., Mayeda, A., & Kozak, D. (1991). Functional Expression of Cloned Human Splicing
817 Factor SF2: Homology to RNA-Binding Proteins, Ul 70K, and Drosophila Splicing
818 Regulators. *Cell*, *66*, 383–394.
819 Kuleshov, M. V., Jones, M. R., Rouillard, A. D., Fernandez, N. F., Duan, Q., Wang, Z., Koplev,
820 S., Jenkins, S. L., Jagodnik, K. M., Lachmann, A., McDermott, M. G., Monteiro, C. D.,
821 Gundersen, G. W., & Ma'ayan, A. (2016). Enrichr: A comprehensive gene set
822 enrichment analysis web server 2016 update. *Nucleic Acids Research*, *44*(W1), W90–
823 W97. https://doi.org/10.1093/nar/gkw377
824 Lee, S., Sears, M. J., Zhang, Z., Li, H., Salhab, I., Krebs, P., Xing, Y., Nah, H.-D., Williams, T., &
825 Carstens, R. P. (2020). Cleft lip and cleft palate in *Esrp1* knockout mice is associated
826 with alterations in epithelial-mesenchymal crosstalk. *Development*, *147*(21), dev187369.
827 https://doi.org/10.1242/dev.187369

828 Li, D., & Roberts, R. (2001). WD-repeat proteins: Structure characteristics, biological function,
829 and their involvement in human diseases. *Cellular and Molecular Life Sciences*, *58*.
830 Liao, X., Hu, K., Salhi, A., Zou, Y., Wang, J., & Gao, X. (2022). msRepDB: A comprehensive
831 repetitive sequence database of over 80 000 species. *Nucleic Acids Research*, *50*(D1),
832 D236–D245. https://doi.org/10.1093/nar/gkab1089
833 Licatalosi, D. D., & Darnell, R. B. (2010). RNA processing and its regulation: Global insights into
834 biological networks. *Nature Reviews Genetics*, *11*(1), 75–87.
835 https://doi.org/10.1038/nrg2673
836 Liu, K., Jian, Y., Sun, X., Yang, C., Gao, Z., Zhang, Z., Liu, X., Li, Y., Xu, J., Jing, Y., Mitani, S.,
837 He, S., & Yang, C. (2016). Negative regulation of phosphatidylinositol 3-phosphate
838 levels in early-to-late endosome conversion. *Journal of Cell Biology, 212*(2), 181-198.
839 https://doi.org/10.1083/jcb.201506081.
840 Long, Y., Sou, W. H., Yung, K. W. Y., Liu, H., Wan, S. W. C., Li, Q., Zeng, C., Law, C. O. K.,
841 Chan, G. H. C., Lau, T. C. K., & Ngo, J. C. K. (2019). Distinct mechanisms govern the
842 phosphorylation of different SR protein splicing factors. *Journal of Biological Chemistry*,
843 *294*(4), 1312–1327. https://doi.org/10.1074/jbc.RA118.003392
844 Love, M. I., Huber, W., & Anders, S. (2014). Moderated estimation of fold change and
845 dispersion for RNA-seq data with DESeq2. *Genome Biology*, *15*(12), 550.
846 https://doi.org/10.1186/s13059-014-0550-8
847 Mai, C. T., Isenburg, J. L., Canfield, M. A., Meyer, R. E., Correa, A., Alverson, C. J., Lupo, P. J.,
848 Riehle-Colarusso, T., Cho, S. J., Aggarwal, D., Kirby, R. S., & National Birth Defects
849 Prevention Network. (2019). National population-based estimates for major birth defects,
850 2010–2014. *Birth Defects Research*, *111*(18), 1420–1435.
851 https://doi.org/10.1002/bdr2.1589
852 Manning, B. D., & Cantley, L. C. (2007). AKT/PKB Signaling: Navigating Downstream. *Cell*,
853 *129*(7), 1261–1274. https://doi.org/10.1016/j.cell.2007.06.009

854 Martin, M. (2011). Cutadapt removes adapter sequences from high-throughput sequencing
855 reads. *EMBnet.Journal*, *17*(1), 10. https://doi.org/10.14806/ej.17.1.200
856 Moss, N. D., Wells, K. L., Theis, A., Kim, Y.-K., Spigelman, A. F., Liu, X., MacDonald, P. E., &
857 Sussel, L. (2023). Modulation of insulin secretion by RBFOX2-mediated alternative
858 splicing. *Nature Communications*, *14*(1), 7732. https://doi.org/10.1038/s41467-023-
859 43605-4
860 Pan, Q., Shai, O., Lee, L. J., Frey, B. J., & Blencowe, B. J. (2008). Deep surveying of alternative
861 splicing complexity in the human transcriptome by high-throughput sequencing. *Nature*
862 *Genetics*, *40*(12), 1413–1415. https://doi.org/10.1038/ng.259
863 Park, J. W., Jung, S., Rouchka, E. C., Tseng, Y-T., & Xing, Y. (2016). rMAPS: RNA map
864 analysis and plotting server for alternative exon regulation. *Nucleic Acids Research*
865 *44*(W1), 333-338. https://doi.org/10.1093/nar/gkw410
866 Patro, R., Duggal, G., Love, M. I., Irizarry, R. A., & Kingsford, C. (2017). Salmon provides fast
867 and bias-aware quantification of transcript expression. *Nature Methods*, *14*(4), 417–419.
868 https://doi.org/10.1038/nmeth.4197
869 Ramírez, F., Ryan, D. P., Grüning, B., Bhardwaj, V., Kilpert, F., Richter, A. S., Heyne, S.,
870 Dündar, F., & Manke, T. (2016). deepTools2: A next generation web server for deep-
871 sequencing data analysis. *Nucleic Acids Research*, *44*(W1), W160–W165.
872 https://doi.org/10.1093/nar/gkw257
873 Rapiteanu, R., Davis, L. J., Williamson, J. C., Timms, R. T., Paul Luzio, J., & Lehner, P. J.
874 (2016). A Genetic Screen Identifies a Critical Role for the WDR81-WDR91 Complex in
875 the Trafficking and Degradation of Tetherin. *Traffic*, *17*(8), 940–958.
876 https://doi.org/10.1111/tra.12409
877 Rattanasopha, S., Tongkobpetch, S., Srichomthong, C., Siriwan, P., Suphapeetiporn, K., &
878 Shotelersuk, V. (2012). PDGFRa mutations in humans with isolated cleft palate.

European Journal of Human Genetics, *20*(10), 1058–1062. https://doi.org/10.1038/ejhg.2012.55

Riemondy, K. A., Sheridan, R. M., Gillen, A., Yu, Y., Bennett, C. G., & Hesselberth, J. R. (2017). valr: Reproducible genome interval analysis in R. *F1000Research*, *6*, 1025. https://doi.org/10.12688/f1000research.11997.1

Robinson, J. T., Thorvaldsdóttir, H., Winckler, W., Guttman, M., Lander, E. S., Getz, G., & Mesirov, J. P. (2011). Integrative genomics viewer. *Nature Biotechnology*, *29*(1), 24–26. https://doi.org/10.1038/nbt.1754

Rogers, M. A., Campaña, M. B., Long, R., & Fantauzzo, K. A. (2022). PDGFR dimer-specific activation, trafficking and downstream signaling dynamics. *Journal of Cell Science*, *135*(17), jcs259686. https://doi.org/10.1242/jcs.259686

Schmok, J. C., Jain, M., Street, L. A., Tankka, A. T., Schafer, D., Her, H.-L., Elmsaouri, S., Gosztyla, M. L., Boyle, E. A., Jagannatha, P., Luo, E.-C., Kwon, E. J., Jovanovic, M., & Yeo, G. W. (2024). Large-scale evaluation of the ability of RNA-binding proteins to activate exon inclusion. *Nature Biotechnology*. https://doi.org/10.1038/s41587-023-02014-0

Scotti, M. M., & Swanson, M. S. (2016). RNA mis-splicing in disease. *Nature Reviews Genetics*, *17*(1), 19–32. https://doi.org/10.1038/nrg.2015.3

Shen, H., & Green, M. R. (2006). RS domains contact splicing signals and promote splicing by a common mechanism in yeast through humans. *Genes & Development*, *20*(13), 1755–1765. https://doi.org/10.1101/gad.1422106

Shen, S., Park, J. W., Lu, Z., Lin, L., Henry, M. D., Wu, Y. N., Zhou, Q., & Xing, Y. (2014). rMATS: Robust and flexible detection of differential alternative splicing from replicate RNA-Seq data. *Proceedings of the National Academy of Sciences*, *111*(51), E5593–E5601. https://doi.org/10.1073/pnas.1419161111

904 Shin, C., Feng, Y., & Manley, J. L. (2004). Dephosphorylated SRp38 acts as a splicing
905 repressor in response to heat shock. *Nature*, *427*(6974), 553–558.
906 https://doi.org/10.1038/nature02288
907 Simpson, J. E., Muir, M. T., Lee, M., Naughton, C., Gilbert, N., Pollard, S. M., & Gammoh, N.
908 (2024). Autophagy supports PDGFRA-dependent brain tumor development by
909 enhancing oncogenic signaling. *Developmental Cell*, S1534580723006214.
910 https://doi.org/10.1016/j.devcel.2023.11.023
911 Soneson, C., Love, M. I., & Robinson, M. D. (2016). Differential analyses for RNA-seq:
912 Transcript-level estimates improve gene-level inferences [version 2; referees: 2
913 approved]. *F1000Research*, *4*, 1521. https://doi.org/10.12688/F1000RESEARCH.7563.2
914 Soriano, P. (1997). The PDGFα receptor is required for neural crest cell development and for
915 normal patterning of the somites. *Development*, *124*, 2691–2700.
916 Tallquist, M. D., & Soriano, P. (2003). Cell autonomous requirement for PDGFRα in populations
917 of cranial and cardiac neural crest cells. *Development*, *130*(3), 507–518.
918 https://doi.org/10.1242/dev.00241
919 Uyar, B., Yusuf, D., Wurmus, R., Rajewsky, N., Ohler, U., & Akalin, A. (2017). RCAS: An RNA
920 centric annotation system for transcriptome-wide regions of interest. *Nucleic Acids*
921 *Research*, *45*(10), e91–e91. https://doi.org/10.1093/nar/gkx120
922 Van Nostrand, E. L., Nguyen, T. B., Gelboin-Burkhart, C., Wang, R., Blue, S. M., Pratt, G. A.,
923 Louie, A. L., & Yeo, G. W. (2017). Robust, Cost-Effective Profiling of RNA Binding
924 Protein Targets with Single-end Enhanced Crosslinking and Immunoprecipitation
925 (seCLIP). In Y. Shi (Ed.), *mRNA Processing* (Vol. 1648, pp. 177–200). Springer New
926 York. https://doi.org/10.1007/978-1-4939-7204-3_14
927 Van Nostrand, E. L., Pratt, G. A., Shishkin, A. A., Gelboin-Burkhart, C., Fang, M. Y.,
928 Sundararaman, B., Blue, S. M., Nguyen, T. B., Surka, C., Elkins, K., Stanton, R., Rigo,
929 F., Guttman, M., & Yeo, G. W. (2016). Robust transcriptome-wide discovery of RNA-

binding protein binding sites with enhanced CLIP (eCLIP). *Nature Methods*, *13*(6), 508–514. https://doi.org/10.1038/nmeth.3810

Vasudevan, H. N., Mazot, P., He, F., & Soriano, P. (2015). Receptor tyrosine kinases modulate distinct transcriptional programs by differential usage of intracellular pathways. *eLife*, *4*, e07186. https://doi.org/10.7554/eLife.07186

Wallroth, A., & Haucke, V. (2018). Phosphoinositide conversion in endocytosis and the endolysosomal system. *Journal of Biological Chemistry*, *293*(5), 1526–1535. https://doi.org/10.1074/jbc.R117.000629

Wang, E. T., Sandberg, R., Luo, S., Khrebtukova, I., Zhang, L., Mayr, C., Kingsmore, S. F., Schroth, G. P., & Burge, C. B. (2008). Alternative isoform regulation in human tissue transcriptomes. *Nature*, *456*(7221), 470–476. https://doi.org/10.1038/nature07509

Xiao, S.-H., & Manley, J. (1997). Phosphorylation of the ASF/SF2 RS domain affects both protein-protein and protein-RNA interactions and is necessary for splicing. *Genes & Development*, 12.

Zahler, A. M., Neugebauer, K. M., Lane, W. S., & Roth, M. B. (1993). Distinct Functions of SR Proteins in Alternative pre-mRNA Splicing. *Science*, *260*(5105), 219–222. https://doi.org/10.1126/science.8385799

Zerial, M., & McBride, H. (2001). Rab proteins as membrane organizers. *Nature Reviews Molecular Cell Biology*, *2*(2), 107–117. https://doi.org/10.1038/35052055

Zhou, Z., & Fu, X.-D. (2013). Regulation of splicing by SR proteins and SR protein-specific kinases. *Chromosoma*, *122*(3), 191–207. https://doi.org/10.1007/s00412-013-0407-z

Zhou, Z., Qiu, J., Liu, W., Zhou, Y., Plocinik, R. M., Li, H., Hu, Q., Ghosh, G., Adams, J. A., Rosenfeld, M. G., & Fu, X.-D. (2012). The Akt-SRPK-SR Axis Constitutes a Major Pathway in Transducing EGF Signaling to Regulate Alternative Splicing in the Nucleus. *Molecular Cell*, *47*(3), 422–433. https://doi.org/10.1016/j.molcel.2012.05.014

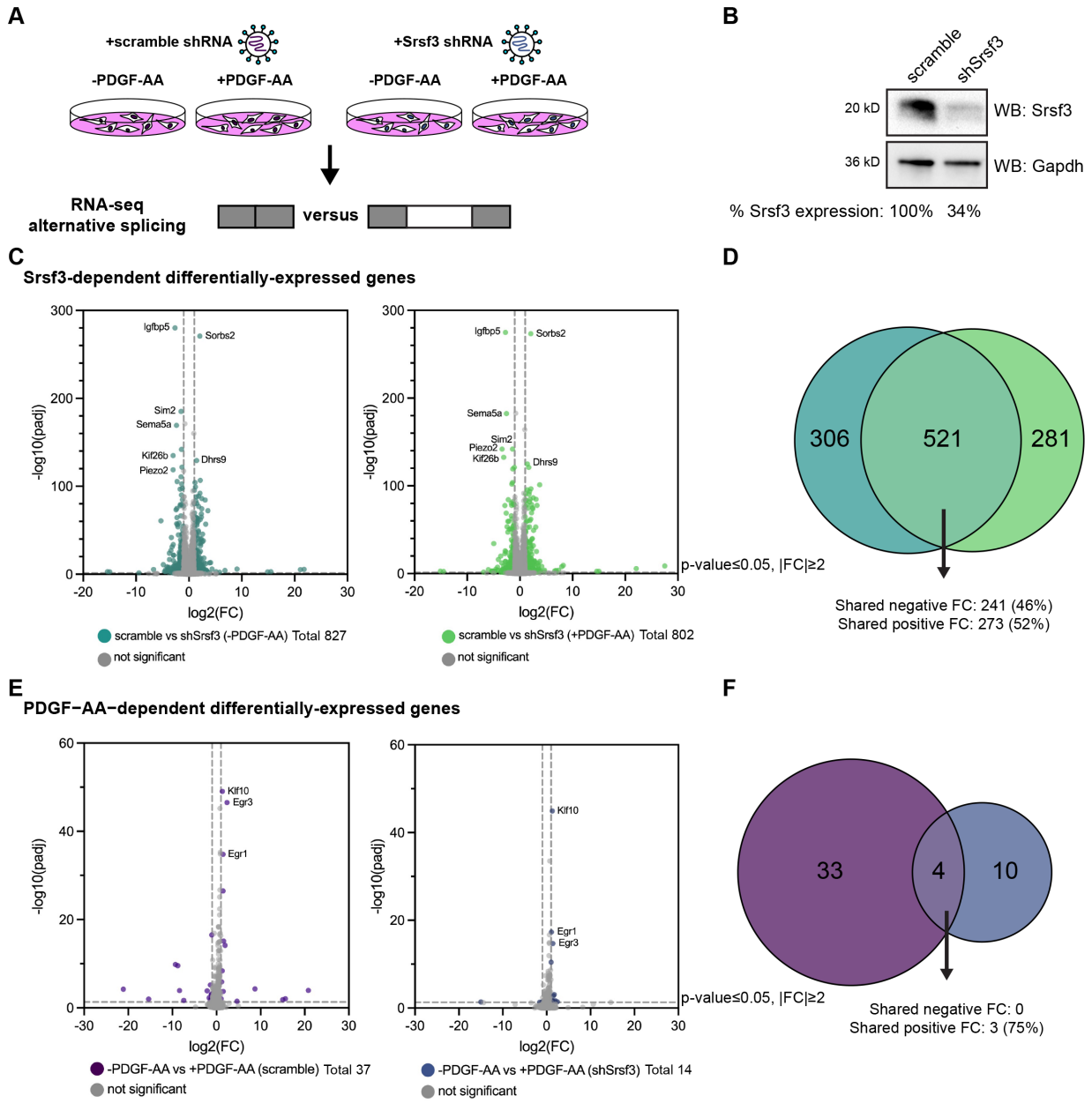

Figure 1: PDGFRα signaling for one hour minimally affects gene expression. (A) Schematic of RNA-seq experimental design. iMEPM cells were transduced to stably express a scramble shRNA (scramble) or shRNA targeting the 3' UTR of *Srsf3* (shSrsf3). iMEPM cells expressing either scramble or shSrsf3 were left unstimulated or stimulated with 10 ng/mL PDGF-AA for 1 hour and RNA was isolated for RNA-seq analysis. **(B)** Western blot (WB) analysis of whole-cell lysates from scramble and shSrsf3 cell lines with anti-Srsf3 and anti-

963 Gapdh antibodies. The percentage of Srsf3 expression normalized to Gapdh expression is
964 indicated below. **(C)** Volcano plots depicting differentially-expressed genes in scramble versus
965 shSrsf3 cell lines in the absence (left) or presence (right) of PDGF-AA stimulation. Log_2(fold
966 change) (FC) values represent log_2(shSrsf3 normalized counts/scramble normalized counts).
967 Significant changes in gene-level expression are reported for genes with adjusted *P* (padj) <
968 0.05 and fold change |FC| ≥ 2. **(D)** Venn diagram of significant genes from C. **(E)** Volcano plots
969 depicting differentially-expressed genes in the absence versus presence of PDGF-AA ligand in
970 scramble (left) or shSrsf3 (right) cell lines. Log_2(FC) values represent log_2(+PDGF-AA
971 normalized counts/-PDGF-AA normalized counts). **(F)** Venn diagram of significant genes from
972 E.
973

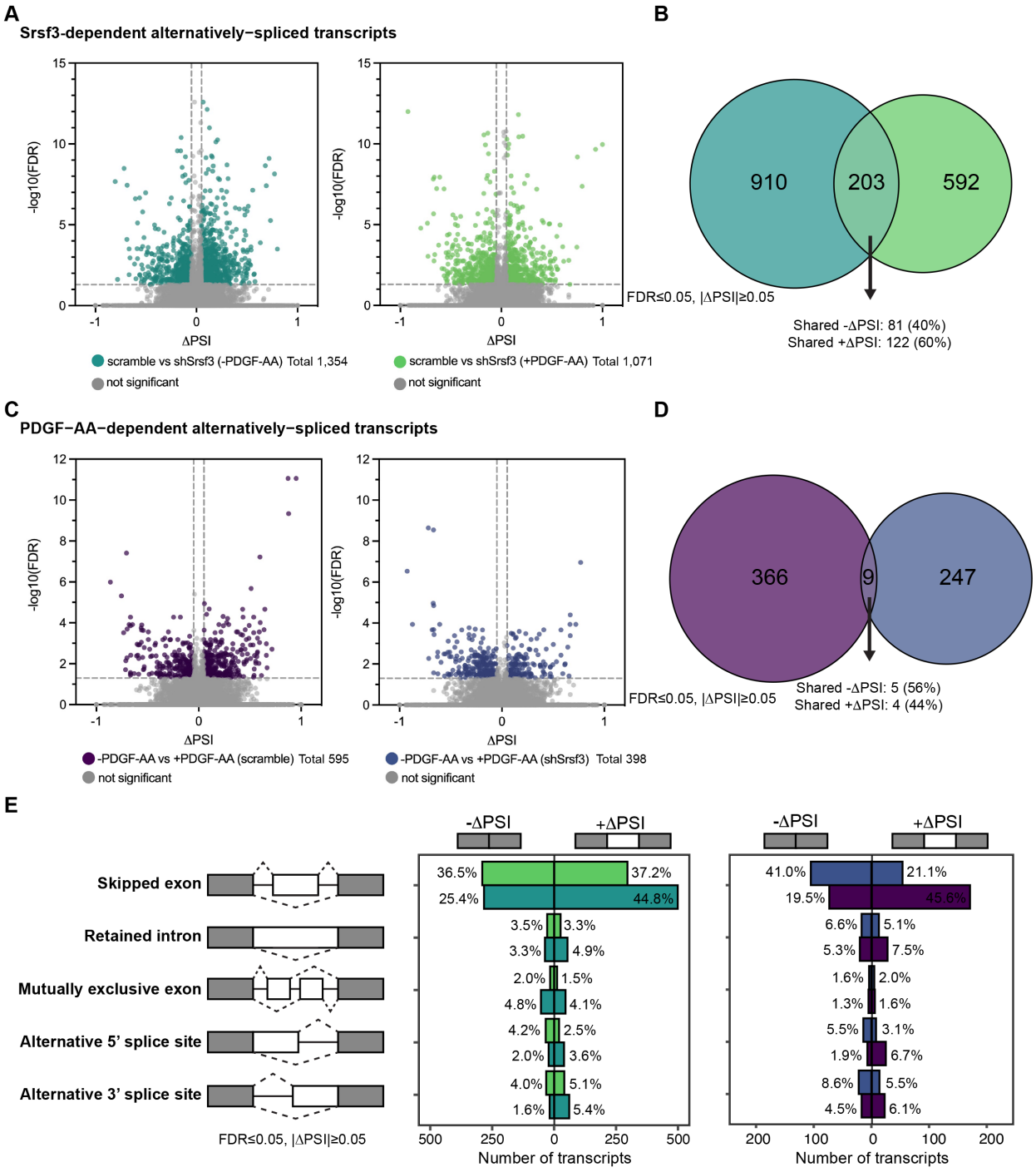

Figure 2: PDGFRα signaling for one hour has a more pronounced effect on alternative RNA splicing. (A) Volcano plots depicting alternatively-spliced transcripts in scramble versus shSrsf3 cell lines in the absence (left) or presence (right) of PDGF-AA stimulation. Difference in percent spliced in (ΔPSI) values represent scramble PSI – shSrsf3 PSI. Significant changes in

979 alternative RNA splicing are reported for events with a false discovery rate (FDR) $\leq$ 0.05 and a
980 difference in percent spliced in (|ΔPSI|) $\geq$ 0.05. **(B)** Venn diagram of significant transcripts from
981 A, filtered to include events detected in at least 10 reads in either condition. **(C)** Volcano plots
982 depicting alternatively-spliced transcripts in the absence versus presence of PDGF-AA ligand in
983 scramble (left) or shSrsf3 (right) cell lines. Difference in percent spliced in (ΔPSI) values
984 represent -PDGF-AA PSI – +PDGF-AA PSI. **(D)** Venn diagram of significant transcripts from C,
985 filtered to include events detected in at least 10 reads in either condition. **(E)** Bar graph
986 depicting alternative RNA splicing events in scramble versus shSrsf3 cell lines in the absence or
987 presence of PDGF-AA stimulation (left) or in the absence versus presence of PDGF-AA ligand
988 in scramble or shSrsf3 cell lines (right).
989

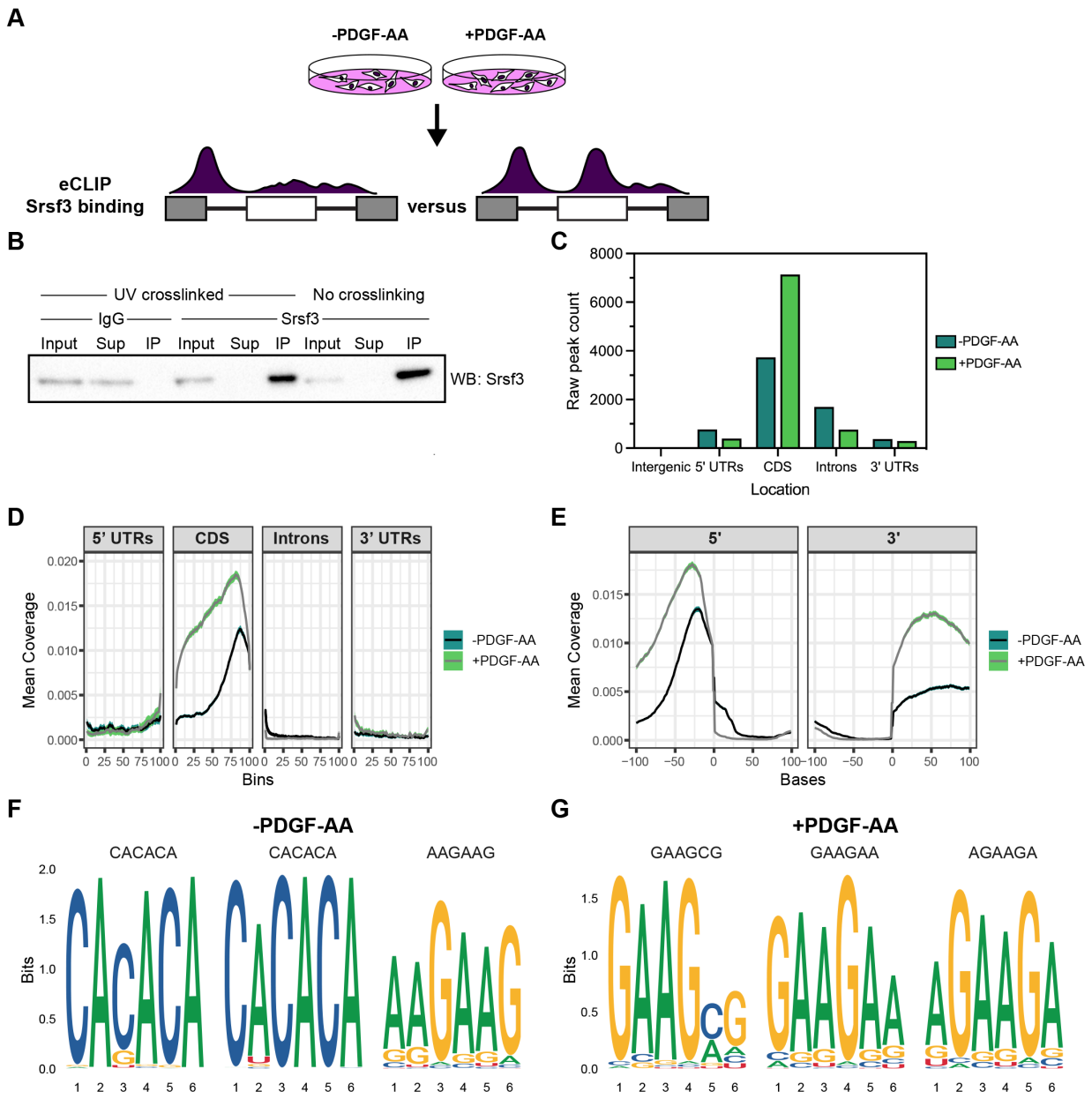

Figure 3: Srsf3 exhibits differential transcript binding upon PDGFRα signaling. (A) Schematic of eCLIP experimental design. iMEPM cells were left unstimulated or stimulated with 10 ng/mL PDGF-AA for 1 hour and processed for eCLIP analysis. **(B)** Immunoprecipitation (IP) of Srsf3 from cells that were UV-crosslinked or not UV-crosslinked with IgG or an anti-Srsf3 antibody followed by western blotting (WB) of input, supernatant (Sup), and IP samples with an anti-Srsf3 antibody. **(C)** Mapping of eCLIP peaks to various transcript locations in the absence or presence of PDGF-AA stimulation. 5' UTR, 5' untranslated region; CDS, coding sequence; 3'

998 UTR, 3' untranslated region. **(D,E)** Mean coverage of eCLIP peaks across various transcript
999 locations (D) and surrounding the 5' and 3' splice sites (E) in the absence or presence of PDGF-
1000 AA stimulation. **(F,G)** Top three motifs enriched in eCLIP peaks in the absence (F) or presence
1001 (G) of PDGF-AA stimulation.
1002

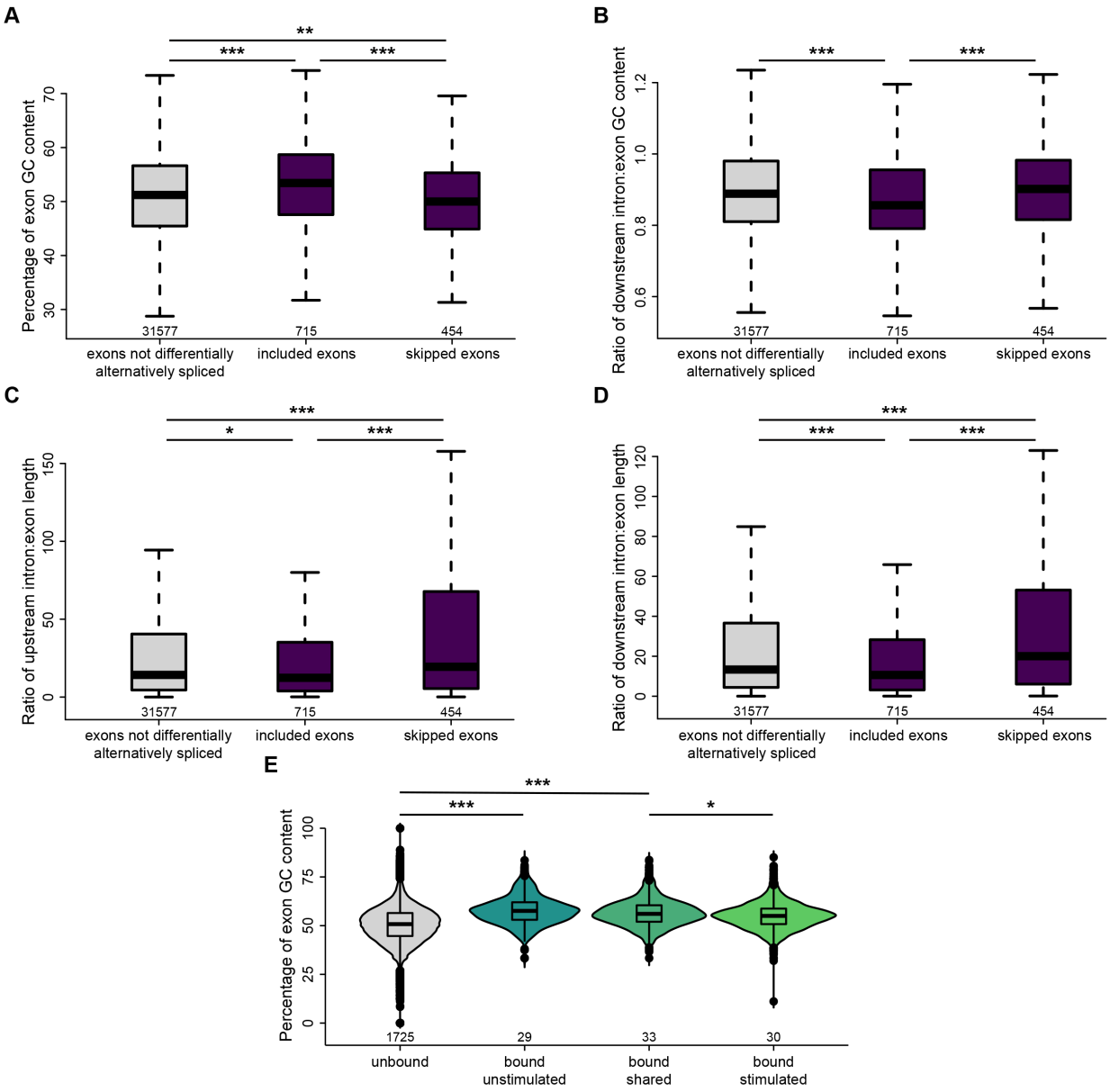

1003

1004 **Figure 4: Srsf3 and PDGFRα signaling are associated with differential GC content and**

1005 **length of alternatively-spliced exons. (A)** Box and whisker plot depicting the percentage of

1006 exon GC content in exons that are not differentially alternatively spliced, and exons that are

1007 included or skipped when Srsf3 is present from the rMATS analysis. **(B)** Box and whisker plot

1008 depicting the ratio of downstream intron to exon GC content in exons that are not differentially

1009 alternatively spliced, and exons that are included or skipped when Srsf3 is present from the

1010 rMATS analysis. **(C,D)** Box and whisker plots depicting the ratio of upstream intron to exon

1011 length (C) and downstream intron to exon length (D) in exons that are not differentially
1012 alternatively spliced, and exons that are included or skipped when Srsf3 is present from the
1013 rMATS analysis. **(E)** Violin and box and whisker (inset) plots depicting the percentage of exon
1014 GC content in exons that are not bound by Srsf3, and exons that are bound in the absence
1015 and/or presence of PDGF-AA stimulation from the eCLIP analysis. *, $P < 0.05$; **, $P < 0.01$; ***,
1016 $P < 0.001$.
1017

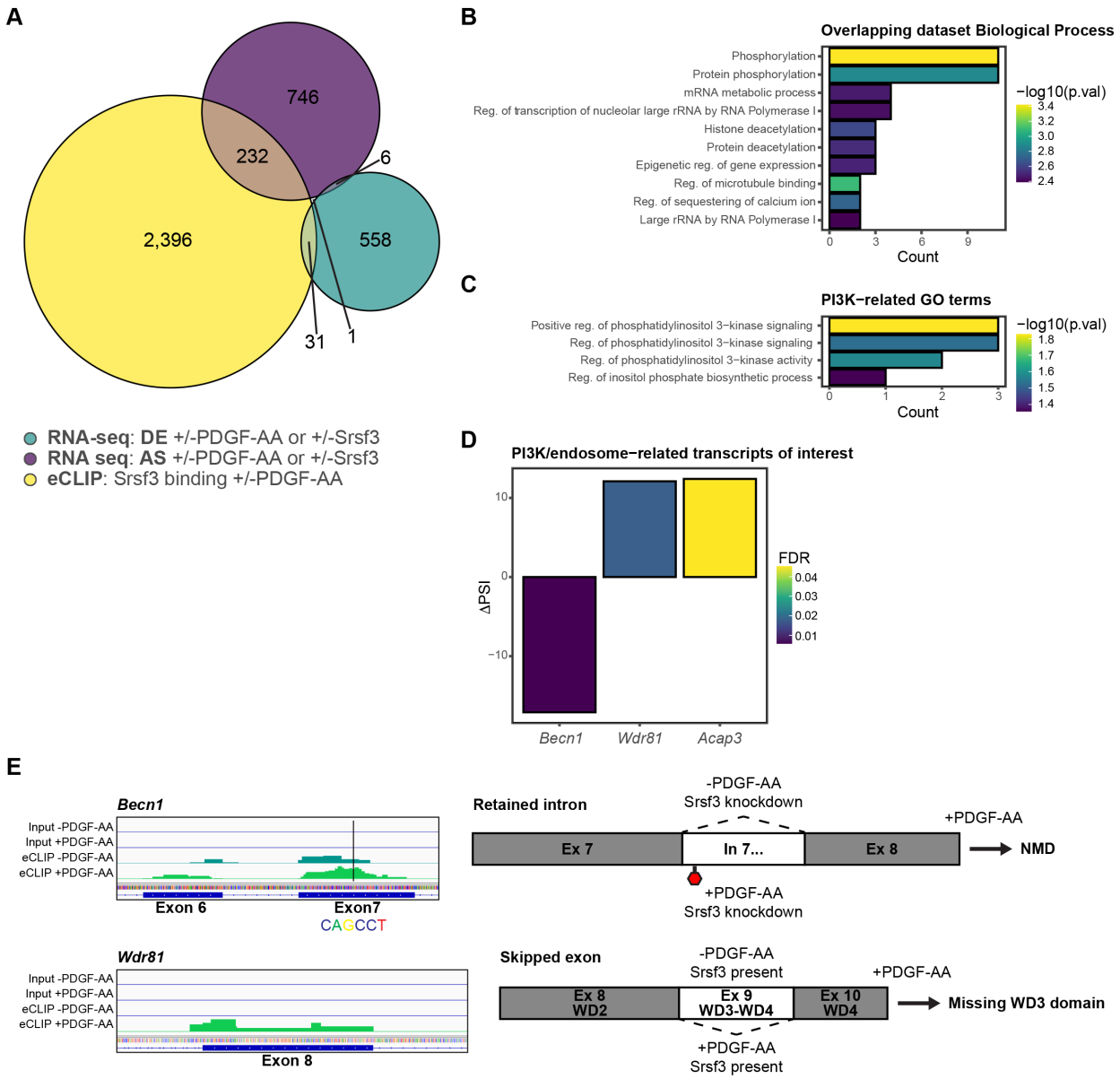

Figure 5: Transcripts bound by Srsf3 that undergo alternative splicing upon PDGFRα signaling encode regulators of PI3K signaling. (A) Venn diagram of genes with differential expression (DE) or transcripts subject to alternative RNA splicing (AS) across the four treatment comparisons that overlap with transcripts with Srsf3 eCLIP peaks in the absence or presence of PDGF-AA stimulation. **(B,C)** Top ten (B) and PI3K-related (C) biological process gene ontology (GO) terms for transcripts from the overlapping datasets. p.val, *P*. **(D)** Difference in percent spliced in (ΔPSI) values for PI3K/endosome-related transcripts of interest. FDR, false detection

1026 rate. **(E)** Peak visualization for input and eCLIP samples in the absence or presence of PDGF-
1027 AA stimulation from Integrative Genomics Viewer (left) with location of motifs from Figure S5
1028 indicated below for PI3K/endosome-related transcripts of interest. Predicted alternative splicing
1029 outcomes for PI3K/endosome-related transcripts of interest (right).
1030

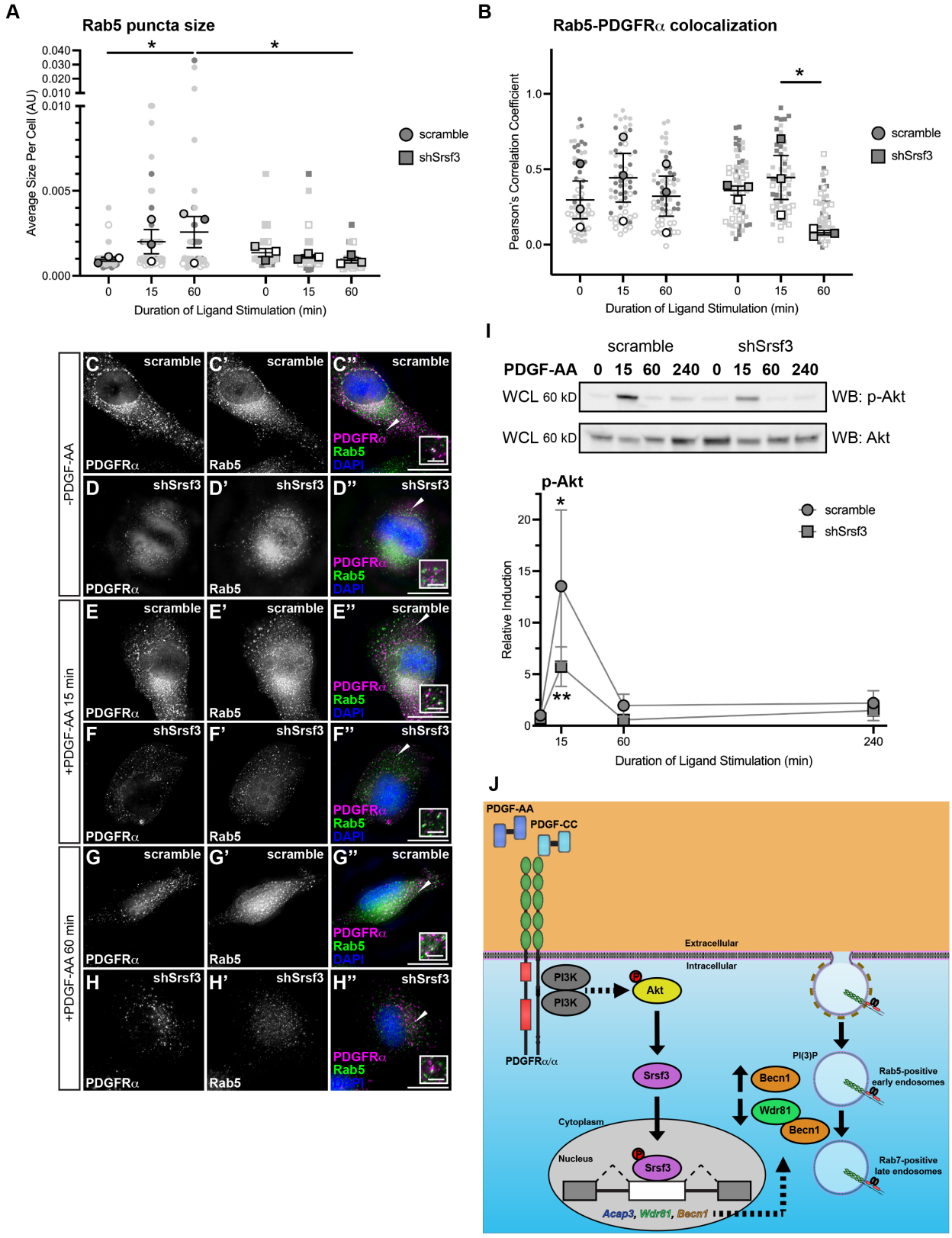
A
Rab5 puncta size
Average Size Per Cell (AU)
Duration of Ligand Stimulation (min)
scramble
shSrsf3
B
Rab5-PDGFRα colocalization
Pearson's Correlation Coefficient
Duration of Ligand Stimulation (min)
scramble
shSrsf3
-PDGF-AA
+PDGF-AA 15 min
+PDGF-AA 60 min
PDGFRα
Rab5
DAPI
I
scramble
shSrsf3
PDGF-AA 0 15 60 240 0 15 60 240
WCL 60 kD
WB: p-Akt
WB: Akt
p-Akt
Relative Induction
Duration of Ligand Stimulation (min)
J
PDGF-AA
PDGF-CC
Extracellular
Intracellular
PI3K
Akt
PDGFRα/α
Srsf3
Cytoplasm
Nucleus
Acap3, Wdr81, Becn1
Becn1
Wdr81
PI(3)P
Rab5-positive early endosomes
Rab7-positive late endosomes

1031

1032 **Figure 6: Srsf3 regulates early endosome size and phosphorylation of Akt downstream of**
1033 **PDGFRα signaling. (A,B)** Scatter dot plots depicting average size of Rab5 puncta per cell (A)
1034 and Pearson's correlation coefficient of signals from anti-Rab5 and anti-PDGFRα antibodies (B)
1035 in scramble and shSrsf3 cell lines in the absence or presence (15-60 min) of PDGF-AA
1036 stimulation. Data are mean ± s.e.m. *, $P < 0.05$. Shaded shapes correspond to independent
1037 experiments. Summary statistics from biological replicates consisting of independent
1038 experiments (large shapes) are superimposed on top of data from all cells; $n = 20$ technical
1039 replicates across each of three biological replicates. **(C-H")** PDGFRα antibody signal (white or
1040 magenta) and Rab5 antibody signal (white or green) as assessed by immunofluorescence
1041 analysis of scramble and shSrsf3 cells in the absence or presence (15-60 min) of PDGF-AA
1042 stimulation. Nuclei were stained with DAPI (blue). White arrows denote colocalization. Scale
1043 bars: 20 μm (main images), 3 μm (insets). **(I)** Western blot (WB) analysis of whole-cell lysates
1044 (WCL) from scramble (left) and shSrsf3 (right) cell lines following a time course of PDGF-AA
1045 stimulation from 15 min to 4 h, with anti-phospho-(p)-Akt and anti-Akt antibodies. Line graphs
1046 depicting quantification of band intensities from $n = 3$ biological replicates as above. Data are
1047 mean ± s.e.m. *, $P < 0.05$; **, $P < 0.01$. **(J)** Model of experimental results in which PI3K/Akt-
1048 mediated PDGFRα signaling results in the nuclear translocation of Srsf3 and the subsequent
1049 AS of transcripts to decrease levels of proteins that promote PDGFRα trafficking out of early
1050 endosomes.